Discovery of BUB1 kinase inhibitors for the treatment of cancer

Bosman, R.E.J.

6

Profiling of benzimidazole-based BUB1 inhibitors

Introduction

Eukaryotic cell division proceeds through four consecutive phases, one of which is mitosis. During mitosis, duplicated genetic material must be equally divided among the newly formed daughter cells. To accurately separate sister chromatids, microtubules emanating from the spindle poles must form bi-oriented attachments with kinetochores which are located at the centromeres of these chromatids.[1] Proper attachment is important for genomic integrity since mitotic progression with attachment errors can lead to gain and loss of chromosomes. An abnormal number of chromosomes, a state referred to as aneuploidy, is thought to contribute to tumorigenesis.[2] The process of forming correct kinetochore-microtubule attachments is therefore carefully monitored by a safety mechanism called the spindle assembly checkpoint (SAC). The SAC prevents mitotic progression to the anaphase before all chromosomes are correctly attached to the mitotic spindle.[3] Proper SAC functioning is therefore crucial for cell division and survival. As a result, interfering with the SAC and impairing chromosome segregation, has emerged as potential anti-cancer strategy.[2,4] Key proteins of the SAC, including kinases such as monopolar spindle 1 (MPS1) and budding uninhibited by benzimidazole 1 (BUB1), may therefore be interesting therapeutic targets.[2,4]

Taxanes are a class of microtubule targeting drugs, including paclitaxel and docetaxel, that are used for the treatment of various types of cancer, such as ovarian, breast and non-small cell lung cancer.[5,6] Taxane-based chemotherapy is usually associated with severe adverse effects, including bone marrow suppression, peripheral neuropathy and hypersensitivity reactions.[7] Lowering taxane exposure during anti-cancer therapy is therefore desired. Previously, it has been shown that genetically reducing MPS1 levels sensitized several cancer cell lines, including U2OS cells, to low doses (1 – 10 nM) of paclitaxel.[8] In line with these findings, another report showed that the efficacy of docetaxel could be enhanced by pharmacological MPS1 inhibition using small molecule NTRC0066-0 in a mouse xenograft model of human triple-negative breast cancer.[9] Similarly, a small molecule inhibitor of BUB1, BAY1816032 (**Figure 6.1**), was reported to synergistically inhibit a panel of cancer cell lines when combined with taxanes.[10] In a mouse xenograft model this combination of BUB1 inhibition and paclitaxel showed promising anti-tumor effects. Importantly, the combination therapy reduced tumor growth, but BAY1816032 as single agent treatment did not show efficacy *in vivo*. The reason for this is currently unknown, but low amounts of BUB1 protein are thought to be sufficient for proper SAC functioning.[11] Thus, incomplete BUB1 target engagement by BAY1816032 may explain its lack of efficacy as a single agent. The discovery of novel BUB1 inhibitors with the ability to exhibit full target engagement is, therefore, desired to test this hypothesis. Improving the physicochemical properties of compounds to increase their cell permeability may contribute to better target engagement. In addition, frequent exposure to kinase inhibitors may induce mutations in the target protein which prevent inhibitor binding.[12] To overcome this acquired drug resistance, additional chemotypes are warranted.

In **Chapter 4** a series of substituted 2-phenyl-5-methoxy-*N*-(3-(5-(morpholinomethyl)-1*H*-benzo[*d*]imidazol-2-yl)-1*H*-pyrazol-4-yl)pyrimidin-4-amines were discovered as highly potent BUB1 kinase inhibitors with half maximal inhibitory concentrations (IC_{50} values) ranging from 2 – 30 nM. A subset of these molecules matched or even exceeded the biochemical potency of BAY1816032. This chapter describes the further profiling of these inhibitors in absorption, distribution, metabolism and excretion (ADME) assays, cellular BUB1 target engagement and cell proliferation. In addition, the *in vitro* selectivity profile of the most promising inhibitors was assessed and the anti-proliferative activity of one molecule was evaluated in a large panel of cancer cell lines. This led to the identification of ROB433, which showed potent BUB1 target engagement and inhibited a multitude of cancer cell lines as single agent.

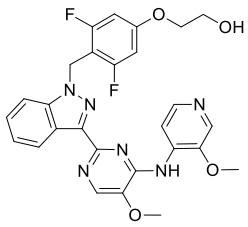

BAY1816032

Figure 6.1 | Chemical structure of BAY1816032.

Results & Discussion

Compounds **1** – **16** (**Table 6.2**) were selected for further biological profiling, because they were the most potent BUB1 inhibitors identified in **Chapter 4**.

Assessment of *in vitro* ADME properties

To investigate the drug-like properties of this chemical series, aqueous solubility and several *in vitro* ADME parameters, such as plasma and microsomal stability and plasma protein binding, were measured of a subset of these molecules (**4** – **9** and **11** – **16**, **Table 6.1**). The stability in both human and rat plasma was good for most compounds. Only compounds **4** and **8** showed a reduced plasma stability (<80% remaining after 3 h). Overall, the human and rat microsomal stability was moderate to good, except for compound **9**. The stability in mouse microsomes was significantly lower for almost all compounds. Compound **11** had the lowest clearance among all species. Of note, this compound did not contain a fluorine at the R_1 phenyl group and increasing the number of fluorine atoms on this ring seemed to lower the metabolic stability. Plasma protein binding was high for all compounds, which correlated with the low to moderate solubility of the compounds. Remarkably, compounds with a hydrogen at R_2 (**4**, **6**, **12**, **14**) were in general better soluble compared to compounds which had a methoxy group at this position (**5**, **7**, **13**, **15**). Taken together, the ADME properties of most of the compounds were acceptable to good.

Table 6.1 | Overview of biochemical pIC_{50} values as determined in **Chapter 4**, *in vitro* ADME parameters and aqueous solubility of compound **4** – **9** and **11** – **16**.

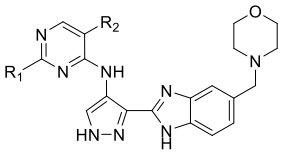

ID	R_1	R_2	pIC_{50} ± SEM	Species	Plasma stability (% remaining after 180 min)	Microsomal stability ($t_{1/2}$ (min))	Microsomal stability (Cl_{int} (µL min^{-1} mg^{-1}))	Plasma protein binding (%)	Aqueous solubility (µM)
4	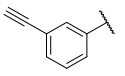		7.57 ± 0.01	Human	76	74	4.7	99.6	
				Rat	100	82	17	99.6	37
				Mouse	N.D.	16	22	N.D.	
5	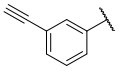		8.37 ± 0.02	Human	100	49	7.1	100	
				Rat	100	64	22	100	5.7
				Mouse	N.D.	30	11	N.D.	
6	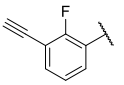		7.89 ± 0.01	Human	100	28	12	99.3	
				Rat	85	29	48	99.1	69
				Mouse	N.D.	16	22	N.D.	
7	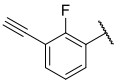		8.34 ± 0.02	Human	100	38	9.1	99.8	
				Rat	91	31	45	99.7	5.0
				Mouse	N.D.	11	33	N.D.	
8	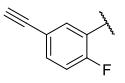		8.68 ± 0.02	Human	69	37	9.4	100	
				Rat	100	49	28	100	3.9
				Mouse	N.D.	18	20	N.D.	
9	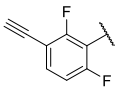		8.64 ± 0.02	Human	100	13	28	99.6	
				Rat	100	35	39	99.7	5.4
				Mouse	N.D.	8.4	41	N.D.	
11	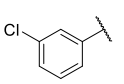		7.96 ± 0.02	Human	100	99	3.5	100	
				Rat	100	75	19	100	1.8
				Mouse	N.D.	73	4.8	N.D.	
12	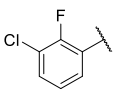		7.63 ± 0.02	Human	100	27	13	99.3	
				Rat	100	46	30	99.2	46
				Mouse	N.D.	12	28	N.D.	
13	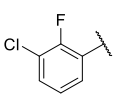		7.98 ± 0.02	Human	86	34	10	99.9	
				Rat	80	34	41	99.8	25
				Mouse	N.D.	12	30	N.D.	
14	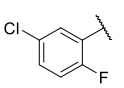		8.03 ± 0.01	Human	100	61	5.6	99.6	
				Rat	96	68	21	99.4	56
				Mouse	N.D.	19	18	N.D.	
15	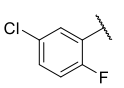		8.57 ± 0.02	Human	100	41	8.4	100	
				Rat	100	63	22	100	4.4
				Mouse	85	22	16	99.9	
16	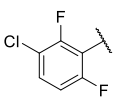		8.62 ± 0.03	Human	100	29	12	99.7	
				Rat	100	49	28	99.7	6.0
				Mouse	N.D.	6.1	57	N.D.	

N.D. = not determined

Assessment of BUB1 target engagement in living cells

To investigate whether the inhibitors engaged with BUB1 in living cells, the inhibitors were profiled in the target engagement assay developed in **Chapter 5**. Compounds **8**, **9**, **15** and **16** potently engaged with BUB1 with half maximal target occupancy concentrations (TE_{50}) of 10-30 nM (**Table 6.2**, **Supplementary Figure 6.1** (p. 207)). This was significantly better than for BAY1816032 (TE_{50} = 355 nM). Target engagement values were approximately 14-fold lower compared to corresponding biochemical pIC_{50} values. This observed reduction may be influenced by the different experimental conditions between these assays and also the cell permeability of the compounds can affect target engagement.[13] In addition, inhibitor target residence time may contribute to the observed difference, since target engagement is measured with a probe that covalently binds BUB1, whereas the inhibitors bind reversibly. BUB1 target engagement by BAY1816032 was more than 75-fold lower compared to its biochemical pIC_{50} value, which may be attributed to unfavorable cell permeability of this compound. A Pearson correlation analysis revealed a strong correlation between cellular target engagement and biochemical pIC_{50} values (**Figure 6.2A**, Pearson's r: 0.921, *p*-value: 0.0004). This indicated that target engagement was predominantly driven by the affinities of these inhibitors for BUB1. Overall, potent cellular BUB1 target engagement was observed for most compounds.

Evaluation of antiproliferative activity

Next, the effect of compounds **1** – **16** on U2OS cell proliferation was investigated by a sulforhodamine B (SRB) assay (**Table 6.2**, **Supplementary Figure 6.2**, (p. 208)).[14] SRB is an aminoxanthene dye, which binds stoichiometrically to basic amino acid residues in trichloroacetic acid (TCA)-fixed cells.[15] SRB is extracted from cells and quantified by absorbance measurements.[15] The optical density is proportional to the amount of protein, which is dependent on the number of cells.[15] U2OS cells were incubated for 72 h with different concentrations of inhibitor. To investigate synergistic effects between BUB1 inhibitors and paclitaxel[10], cells were also co-treated with a low dose (4 nM) of paclitaxel in a separate experiment. A Pearson correlation analysis revealed a strong correlation between biochemical activities and pIC_{50} values on cell proliferation (**Figure 6.2B**, Pearson's r: 0.826, *p*-value: <0.0001), however, target engagement and cell proliferation only moderately correlated and lacked statistical significance (**Figure 6.2C**, Pearson's r: 0.655, *p*-value: 0.056). This suggested that inhibition of cell proliferation was, to a large extent, dependent on BUB1 inhibition, but that off-target activity contributed to the observed effect. Compounds **8**, **9** and **16** potently inhibited cell proliferation with IC_{50} values below 100 nM. Of note, paclitaxel cotreatment only significantly increased the activity (fold-change ≥ 1.9) of compounds **1** – **4**, **10**, **12** and **14**, that showed low potency as single agent (pIC_{50} ≤ 6). The most active compound from this subset in combination with paclitaxel treatment (**12**) had a pIC_{50} of 6.45, which did not exceed the activity of the other inhibitors as single agent. Compound **9** was the most active cellular compound with a pIC_{50} of 7.46. Of note, BAY1816032 showed weak inhibitory activity as single agent (pIC_{50} = 5.07), whereas its activity was enhanced 28-fold by

cotreatment with paclitaxel. To summarize, the benzimidazole-based inhibitors showed good cellular activity, which was not further enhanced by cotreatment with paclitaxel.

Table 6.2 | Overview of compounds **1** – **16** and their biochemical half maximal inhibitory concentrations (expressed as pIC_{50} ± SEM, N=2, n=2), cellular half maximal target occupancy concentrations (expressed as pTE_{50} ± SEM, N=3) and half maximal inhibitory concentration on U2OS cell proliferation with (+) and without (-) 4 nM paclitaxel. Corresponding dose-response graphs are reported in **Supplementary Figure 6.1** (target engagement) and **Supplementary Figure 6.2** (SRB assays).

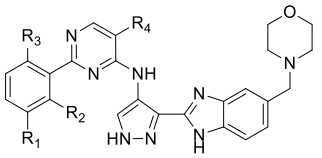

					Biochemical assay			Proliferation assay		
								- paclitaxel	+ paclitaxel	
ID	**R_1**	**R_2**	**R_3**	**R_4**	**pIC_{50} ± SEM**	**app. K_i (nM)[a]**	**pTE_{50} ± SEM**	**pIC_{50} ± SEM**	**pIC_{50} ± SEM**	**f.c.[b]**
BAY-1816032	–	–	–	–	8.34 ± 0.03	1.6	6.45 ± 0.10	5.07 ± 0.05	6.52 ± 0.03	28
1	$-CF_3$	-H	-H	-H	6.03 ± 0.03	329	< 5	~5.4[c]	6.18 ± 0.04	5.4
2	$-CF_3$	-H	-H	-OMe	6.80 ± 0.03	55	N.D.	~6.0[c]	6.32 ± 0.11	2.1
3	-CN	-H	-H	-H	6.24 ± 0.02	201	N.D.	5.56 ± 0.07	6.05 ± 0.08	3.1
4	-C≡C	-H	-H	-H	7.57 ± 0.01	9.5	6.49 ± 0.10	5.70 ± 0.04	6.03 ± 0.08	2.1
5	-C≡C	-H	-H	-OMe	8.37 ± 0.02	1.5	N.D.	6.62 ± 0.05	6.61 ± 0.07	1.0
6	-C≡C	-F	-H	-H	7.89 ± 0.01	4.6	6.24 ± 0.11	6.64 ± 0.05	6.69 ± 0.07	1.1
7	-C≡C	-F	-H	-OMe	8.34 ± 0.02	1.6	7.26 ± 0.08	6.89 ± 0.09	6.91 ± 0.10	1.0
8	-C≡C	-H	-F	-OMe	8.68 ± 0.02	0.74	7.59 ± 0.05	7.13 ± 0.03	7.15 ± 0.05	1.0
9	-C≡C	-F	-F	-OMe	8.64 ± 0.02	0.80	7.54 ± 0.08	7.46 ± 0.05	7.47 ± 0.05	1.0
10	-Cl	-H	-H	-H	7.08 ± 0.02	29	N.D.	5.56 ± 0.01	6.21 ± 0.03	4.5
11	-Cl	-H	-H	-OMe	7.96 ± 0.02	3.9	N.D.	6.26 ± 0.06	6.41 ± 0.07	1.4
12	-Cl	-F	-H	-H	7.63 ± 0.02	8.2	N.D.	5.98 ± 0.05	6.45 ± 0.13	2.9
13	-Cl	-F	-H	-OMe	7.98 ± 0.02	3.7	6.55 ± 0.13	6.73 ± 0.07	6.87 ± 0.08	1.4
14	-Cl	-H	-F	-H	8.03 ± 0.01	3.3	6.75 ± 0.18	5.92 ± 0.06	6.20 ± 0.08	1.9
15 (ROB433)	-Cl	-H	-F	-OMe	8.57 ± 0.02	0.94	7.50 ± 0.11	6.32 ± 0.06	6.48 ± 0.10	1.4
16 (ROB464)	-Cl	-F	-F	-OMe	8.62 ± 0.03	0.84	8.01 ± 0.09	7.39 ± 0.05	7.38 ± 0.05	1.0

[a] apparent K_i ; [b] fold change: increase in activity upon cotreatment with paclitaxel in the SRB assay ($IC_{50\ (+paclitaxel)}$ / $IC_{50\ (-paclitaxel)}$); [c] Due to a steep Hill slope data was reported as ambiguous according to GraphPad Prism; N.D. = not determined.

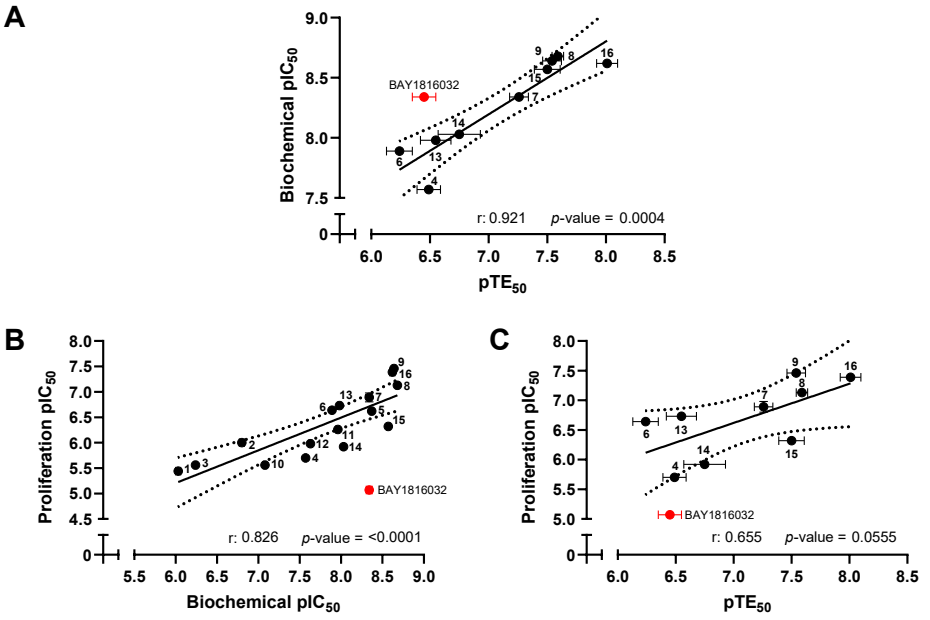

Figure 6.2 | Correlation analysis between **(A)** biochemical pIC_{50} values and pTE_{50} values, **(B)** biochemical pIC_{50} values and pIC_{50} values on cell proliferation and **(C)** pTE_{50} values and pIC_{50} values on cell proliferation. Statistics was performed using a two-tailed Pearson correlation analysis. Biochemical pIC_{50} values are displayed as mean ± SEM (N=2, n=2), pTE_{50} values as mean ± SEM (N=3) and pIC_{50} values on cell proliferation as mean ± SEM (N=2, n=3). For some data points error bars were smaller than the symbol size. Dotted lines represent 95% confidence interval of the best-fit line (solid line) as determined by linear regression analysis. Data for BAY1816032 is indicated in red and is not included in the correlation and linear regression analyses.

Selectivity profile of 15 and 16

Compound ROB433 (**15**) and ROB464 (**16**) were selected based on their biochemical, cellular and ADME profile for further profiling in a kinase selectivity assay. The selectivity profile was assessed using Thermo Fisher Scientific's SelectScreen™ biochemical kinase profiling service in a panel of 403 wild-type kinases (396 unique kinases, see Experimental section). ROB433 and ROB464 were tested at a concentration of 1 µM and 100 nM (**Supplementary Figure 6.3** (p. 209), **Supplementary Table 6.1** (p. 210)). At 1 µM, 165 and 187 kinases were inhibited (>50%) by ROB433 and ROB464, respectively. Of note, although both compounds are structurally similar, significant differences in inhibition were found for a subset of kinases (**Figure 6.3A**). At 100 nM only 49 and 44 kinases were inhibited by ROB433 and ROB464, respectively. 33 off-targets were shared between both compounds (**Figure 6.3B**). Importantly, MPS1 (also known as TTK) was not inhibited, whereas Aurora kinases A, B and C were identified as off-targets of both compounds (**Supplementary Table 6.1** (p. 210)). Other kinases involved in mitosis[4], such as CDK1, Haspin, PLK1, NEK2, NEK6 and NEK9, were not inhibited. In view of the fact that ATP levels in cells are in millimolar range[16–19] compared to micromolar ATP concentrations used in the biochemical assays, it is unknown whether these off-targets will be inhibited in a living cell. Overall, the selectivity profile of both ROB433 and ROB464 is acceptable.

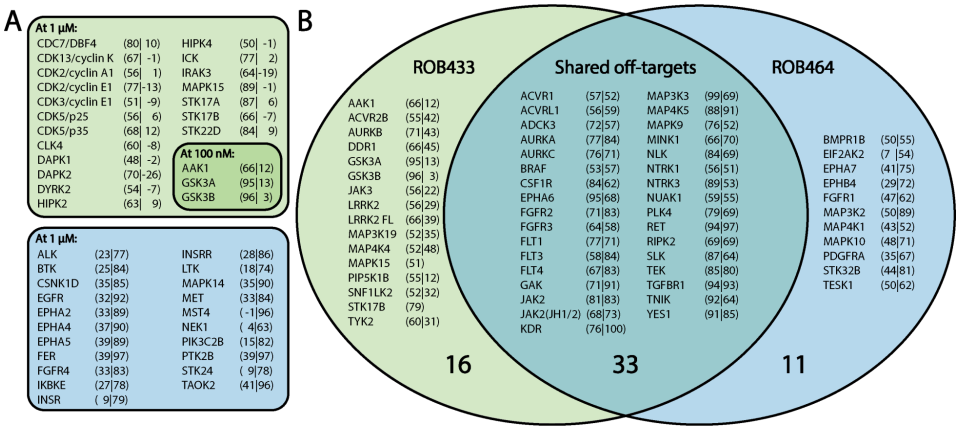

Figure 6.3 | (A) Overview of kinases for which the percentage of inhibition differed ≥50% between ROB433 and ROB464. Kinases that were more prone to inhibition by 1 µM or 100 nM of ROB433 (**15**) compared to corresponding concentrations of ROB464 (**16**) are indicated in the green boxes. Kinases more prominently inhibited by 1 µM ROB464 are indicated in the blue box. Numbers between parentheses indicate percentages of inhibition by ROB433 (left) and ROB464 (right). **(B)** Comparison of *in vitro* selectivity profile of ROB433 and ROB464 at a concentration of 100 nM. Inhibition >50% was used as cut-off. Percentages of inhibition are reported as described in (A). Kinases for which no percentage of inhibition is reported were not inhibited for more than 50% at a concentration of 1 µM and therefore not tested at a concentration of 100 nM. Large numbers indicate the total number of kinases in corresponding part of the Venn diagram.

Antiproliferative effects of ROB433 (15) among a large panel of cancer cell lines

Based on its good biochemical activity and BUB1 target engagement, combined with its acceptable microsomal stability, ROB433 was screened in the Oncolines™ panel which consists of 102 cancer cell lines originating from different tissues (**Supplementary Table 6.2** (p. 212)). Briefly, cells were treated with nine concentrations (3.16 nM – 31.6 µM) of ROB433 for 72 h. Subsequently, cell proliferation was assessed and half maximal inhibitory concentration (IC_{50}), half maximal growth inhibition concentration (GI_{50}) and half maximal lethal dose (LD_{50}) were determined (see Experimental section). ROB433 inhibited cell growth (GI_{50}) with concentrations ranging from 101 nM (for KG-1 cells) to 5.57 µM (for THP-1 cells). Cell lines for which GI_{50}, IC_{50} and LD_{50} values were high, off-target activity may contribute to inhibition of cell proliferation. Cell growth was inhibited with a mean GI_{50} value of 1.43 µM (mean IC_{50} = 1.61 µM) among all cell lines tested which suggested a favorable toxicity profile for this compound. Similar mean IC_{50} values have been published for approved kinase drugs abemaciclib, brigatinib, midostaurin and neratinib (1.71, 1.88, 1.73 and 2.10 µM, respectively) using this Oncolines™ panel.[20] Inhibitors of MPS1 kinase, which is another member of the SAC, have previously been tested in 66 cell lines of the Oncolines™ panel.[21] Among these inhibitors, Mps-BAY2b[22] and tool compound Mps1-12[23] showed similar mean IC_{50} values (1.98 and 1.41 µM, respectively) when compared to ROB433 for this subset of cell lines (mean IC_{50} = 1.63 µM). Classification of cell lines to tissue types and calculating median pIC_{50} values (**Figure 6.4A**) revealed that chronic myeloid leukemia (CML) cells were the most sensitive to ROB433 treatment (median pIC_{50} = 6.10), while non-small cell lung cancer (NSCLC) cells were the least effectively inhibited (median pIC_{50} = 5.53). Strikingly, the opposite was true for cells

treated with MPS1 inhibitors, since low sensitivity was observed for CML cells while NSCLC tissue was in the top 5 most sensitive tissue for seven out of ten MPS1 inhibitors (**Supplementary Figure 6.4**, p. 209).[21] Tissue that was sensitive to both ROB433 and MPS1 inhibitors included uterus and non-hodgkin lymphoma cells (**Supplementary Figure 6.4**, p. 209). To investigate whether certain genomic alterations were related to ROB433 sensitivity, a genomic biomarker analysis was performed on known cancer genes (see Experimental section). This revealed that ROB433 preferentially inhibited proliferation of cells that harbor a mutation in the *CTNNB1* gene (**Figure 6.4B**), which encodes for β-catenin. β-Catenin is a member of the WNT signaling pathway and its accumulation results in nuclear localization and gene transcription.[24] WNT-CTNNB1-dependent transcription ultimately modulates changes in cell behavior, such as cell proliferation.[24] Cell lines with a mutation in the *CTNNB1* gene were on average 2.7-fold more sensitive to ROB433 treatment compared to cells with wild-type *CTNNB1* (ANOVA p = 0.018). Interestingly, this sensitivity was also reported for ten previously investigated MPS1 inhibitors[21], which may be due to targeting the same biological pathway. Cells with an amplification of the *CCNE1* gene, which encodes for cyclin E1, were 2.1-fold less sensitive to ROB433 (**Figure 6.4B**, ANOVA p = 0.029). Cyclin E1 is the regulatory subunit of CDK2 and its gene amplification has been described as a mechanism of primary treatment resistance in serous ovarian cancer.[25] *CCNE1* gene amplification was found to be largely exclusive of *BRCA1/2* pathway disruption.[26] *BRCA1/2*-deficient tumors, which are deficient in homologous recombination (HR) DNA repair, can be targeted by poly (ADP-ribose) polymerase (PARP) inhibitors.[27] PARP inhibitors lead to double-strand DNA breaks which cannot be efficiently repaired in HR deficient cells.[27] It is therefore hypothesized that *CCNE1*-amplified tumors are unlikely to respond to PARP inhibitors.[28] Since BUB1 inhibitor BAY1816032 enhanced the efficacy of PARP inhibitor olaparib a mouse xenograft study[10] and given the reported function of BUB1 in DNA damage response[29], the reduced sensitivity of ROB433 in cells with *CCNE1* gene amplification may therefore be in line with aforementioned data. Overall, ROB433 was found to inhibit a multitude of cancer cell lines originating from different tissues at submicromolar concentrations.

Conclusion

In this chapter, two novel BUB1 inhibitors, ROB433 (**15**) and ROB464 (**16**), are reported. Both compounds showed drug-like *in vitro* ADME properties and inhibited U2OS cell proliferation. In contrast to BAY1816032, the antiproliferative activity of these inhibitors did not require cotreatment with paclitaxel. Potent cellular BUB1 target engagement for ROB433 and ROB464, but less potent for BAY1816032, was observed which supports the hypothesis that full BUB1 inhibition is required to induce antiproliferative activity. Notably, based on the *in vitro* selectivity profiles of ROB433 and ROB464, off-target activity may contribute to the observed cellular effects. The cellular selectivity profile, however, remains to be investigated. The antiproliferative effects of ROB433 were further explored in a large panel of cancer cell lines. ROB433 was able to inhibit a multitude of cell lines, but activity varied among different cancer tissue. Cells with a mutation in the *CTNNB1* gene were found to be more sensitive to

ROB433 treatment, whereas cells with *CCNE1* gene amplification were less affected. Sensitivity to mutations in the *CTNNB1* gene was previously reported for inhibitors of SAC kinase MPS1[21], which may be a result of targeting the same biological pathway. Overall, ROB433 and ROB464 are two novel lead BUB1 inhibitors with favorable properties and provide an excellent expansion of the currently available BUB1 inhibitor BAY1816032.

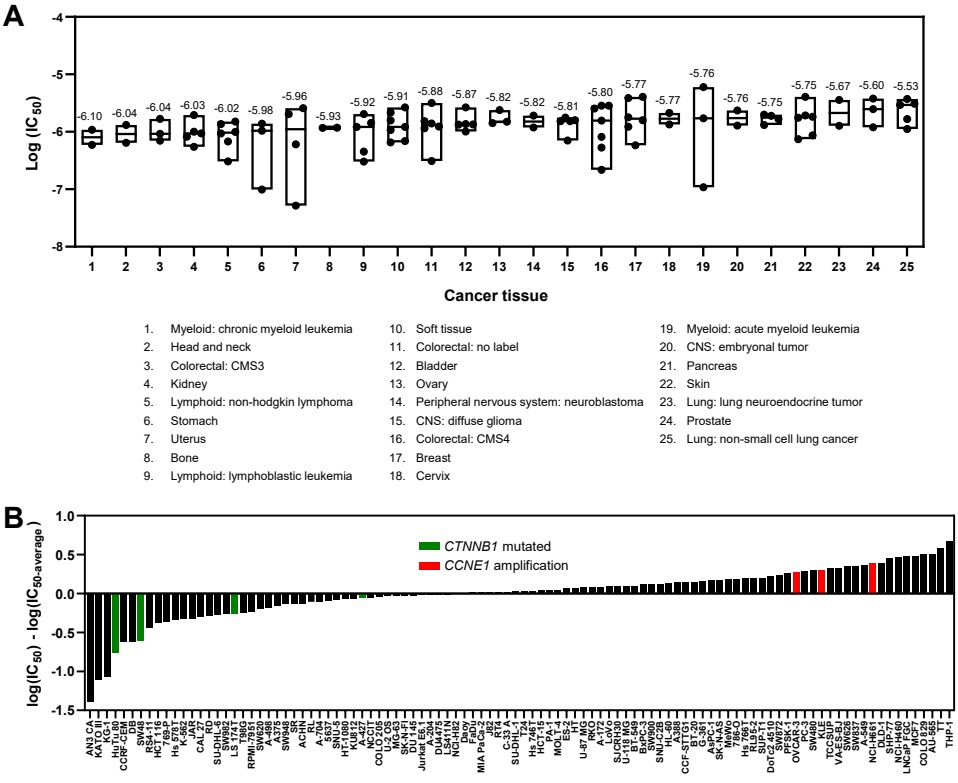

Figure 6.4 | Antiproliferative activity of ROB433 on cancer cells (A) Results of the Oncolines™ profiling service in a panel of 102 cancer cell lines originating from different tissues represented by a tissue-based boxplot (see **Supplementary Table 6.2** (p. 212) for corresponding activity data per cell line). The horizontal line inside each box represents the median log(IC_{50}) value (which is also annotated above each box). **(B)** Waterfall plot raking cell lines on sensitivity. Bars indicate differences from the average pIC_{50} value of the cell panel as: log($IC_{50\_cell\_line}$) – log($IC_{50\_average}$). Bars corresponding to cell lines harboring a *CTNNB1* mutation are indicated in green, cell lines with *CCNE1* gene amplification are indicated in red.

Acknowledgements

From Netherlands Translational Research Center (NTRC), Diep Vu is kindly acknowledged for performing the ADME and solubility assays, Martine Prinsen for conducting the Oncolines™ cell panel screen and Rogier Buijsman for supervision.

Experimental – Biochemistry

Plasma stability assay

Lithium-heparin plasma was thawed and used directly for the assay. An aliquot of 100 µL plasma in a 96-well plate was incubated in a water bath at 37°C for 10 min. Next, 1 µM of compound (max 1% DMSO) or positive control was added and the assay plate was mixed at 1500 rpm for 15 seconds. At 0, 5, 10, 15, 30, 60, 120, 180 min samples of 10 µL were taken and extracted by adding 200 µL of acetonitrile containing an internal standard. The samples were centrifuged for 30 min at 4500 rpm to pellet the precipitated protein and the supernatant was transferred to a True Taper™ 2-mL square 96-well plate (Screening Devices Cat. No. 968820) for LC–MS/MS analysis. Procaine and propantheline were incubated alongside as controls. Procaine is a reference substrate in the rat stability assays, and propantheline in mouse and human stability assays. The signal (counts) was related to the internal standard. Plasma half-life ($t_{1/2}$) was calculated from linear fitting of ln(counts) versus time in Excel. Assay runs were invalidated if $t_{1/2}$ of the controls varied more than two-fold from historical means. The maximum $t_{1/2}$ that could be reliably measured in the assay was determined by analyzing the variation in the replicates of the controls. The percentage remaining compound was calculated by setting the signal at t = 0 to 100%. In addition, %-remaining at 180 min was calculated based on the linear fit used for $t_{1/2}$. The compounds are considered stable if this percentage is higher than 80%.

Microsomal stability assay

The liver microsomal suspensions were thawed and used directly for the assay. To a 96-well plate was added 56 µL of 100 mM KH_2PO_4 (pH 7.4), 2 µL of 50 µg/mL alamethicin, 2 µL of 250 mM $MgCl_2$, 10 µL of liver microsomes and 10 µL of compound (max 1% DMSO) after which the plate was incubated in a water bath at 37°C for 10 min. Next, 20 µL of 10 mM NADPH was added and the assay plate was mixed at 1500 rpm for 15 seconds. At 0, 5, 10, 15, 30, 45, 60, 120 min samples of 10 µL were taken and extracted by adding 200 µL of acetonitrile containing an internal standard. The samples were centrifuged for 30 min at 4000 rpm to pellet the precipitated protein and the supernatant was transferred to a True Taper™ 2-mL square 96-well plate (Screening Devices Cat. No. 968820) for LC–MS/MS analysis. Dextromethorphan, propranolol and phenacetin were incubated alongside as controls. The signal (counts) was related to the internal standard. The half-life ($t_{1/2}$) was calculated from linear fitting of ln(counts) versus time in Excel. Assay runs were invalidated if $t_{1/2}$ or the CL_{int} value of the control compounds varied more than two-fold from historical means.

Plasma protein binding assay

Equilibrium dialysis was used to determine plasma protein binding. DIALYZER™ plates were used that separates a protein-containing compartment from a protein-free compartment via a semi-permeable membrane. The protein-free compartment (clear frame) of the system was filled with 150 µL PBS and the protein-containing side (blue frame) was filled with 150 µL plasma (Sera Laboratories International Ltd. (BioIVT), K_3 EDTA) containing 5 µM of compound (max. 1% DMSO). The filled wells were sealed with cap strips. The system was allowed to rotate for 17 h at 25 rpm, in an incubator at 37°C. After equilibrium had been reached, samples of 10 µL were taken from each of the compartments and extracted by adding 100 µL of acetonitrile containing an internal standard. The samples were centrifuged for 30 min at 4500 rpm to pellet the precipitated protein and the supernatant was transferred to a True Taper™ 2-mL square 96-well plate (Screening Devices Cat. No. 968820) for LC–MS/MS analysis. Tolbutamide was incubated alongside as control. Incubations and subsequent analyses were performed in duplicate. Assay runs were invalidated if the fraction unbound (fu)-value of tolbutamide varied more than two-fold from historical means. The extent of binding is reported as protein binding fraction (PB) which is calculated by PB(%) = 100*(PC – PF)/PC, where PC and PF are the compound concentrations in the protein-containing and protein-free compartments, respectively. The fraction unbound was calculated by fu = 1 – ((PC – PF) /PC).

Solubility assay

Compounds stocks (in DMSO) were diluted in an 8-point dilution series (with a factor 1.67) in DMSO to obtain 33.3x working solutions. In a clear 384-well plate, 3 µL compound from the dilution plate was

added to 10 µL PBS and the plate was mixed at 2000 rpm for 15 seconds. Next, 87 µl PBS was added to the assay plate and mixed 15 times using a Biomek NXP (final concentrations were 14.0, 23.3, 38.9, 64.8, 108, 180, and 300 µM). Absorption was measured at 620 nm using an EnVision® Multimode Plate Reader and the wells were also inspected for turbidity using a microscope. A linear relation between compound concentrations and turbidity signal was fitted and the intersection with the x-axis was determined. This intersection represents the maximal concentration of compound that is supposed to be still in solution. Insoluble compounds were also checked by visual inspection using a microscope.

Cell culture

U2OS (human osteosarcoma) cells were purchased at ATCC and were tested on regular basis for mycoplasma contamination. Cultures were discarded after 2–3 months of use. Cells were cultured at 37°C under 7% CO_2 in DMEM (Sigma Aldrich, D6546) supplemented with GlutaMAX (2 mM, Thermo Fisher), 10% (v/v) heat-inactivated newborn calf serum (Seradigm), penicillin and streptomycin (200 µg/mL each, Duchefa) (complete medium). Growth medium was supplemented with G418 (600 µg/mL) (selection medium) for culturing stable BUB1-overexpressing (U2OS-BUB1^{GFP_FLAG}) cells. U2OS-BUB1^{GFP_FLAG} cells were prepared as described in **Chapter 5**. Medium was refreshed every 2–3 days and cells were passaged by trypsinization twice a week at 80–90% confluence. Cell viability was assessed by Trypan Blue exclusion and cell quantification using a TC20™ Automated Cell Counter (Bio-Rad).

Target engagement assay

U2OS-BUB1^{GFP_FLAG} cells from 10 cm dishes with low cell density (<50% confluence) were seeded into 6-well plates (500,000 cells/well) and incubated overnight to allow for cell adherence. Inhibitor (stock solutions in DMSO) were diluted 100x in complete medium to obtain 10x working solutions (1% DMSO). Inhibitors were serially diluted in complete medium containing 1% DMSO. Cell medium was aspirated and complete medium (800 µL) was added. Either vehicle or inhibitor (100 µL, 10x working solution) was added and cells were incubated at 37°C for 1 h. Vehicle or probe (100 µL, 10x working solution) was added and cells were incubated at 37°C for 1 h. Medium was aspirated and cells were washed with PBS (1 mL). Cells were harvested by trypsinization and centrifuged (500 *g*, 3 min). Pellets were washed with PBS (1 mL), centrifuged (500 *g*, 3 min) and supernatant was removed. Pellets were snap-frozen in liquid nitrogen and subsequently thawed on ice (cell pellets can optionally be stored at –80°C). Cells were lysed by suspending the pellet in 60 µL M-PER™ Mammalian Protein Extraction Reagent (Thermo Fisher), supplemented with 1x Halt™ protease inhibitor cocktail (EDTA-free) (Thermo Fisher) and 1x Halt™ phosphatase inhibitor cocktail (Thermo Fisher), after which the samples were incubated on ice for 15 min. Samples were vortexed at medium speed and centrifuged (14,000 *g*, 10 min, 4°C). The supernatant was collected and protein concentration determined by a Quick Start™ Bradford Protein Assay (Bio-Rad). Lysates were diluted to 1.15 mg/mL in M-PER™ Mammalian Protein Extraction Reagent (lysates can optionally be snap-frozen and stored at –80°C). "Click-mix" was prepared freshly by mixing $CuSO_4$ (42 µL of 15 mM in H_2O) and sodium ascorbate (21 µL of 150 mM in H_2O) until yellow, followed by the addition of THPTA (7 µL of 15 mM in H_2O) and Cy5-N_3 (7 µL of 82.5 µM in DMSO). To 26 µL lysate was added 4 µL click-mix and samples were incubated at 37°C for 30 min. Samples were denatured by the addition of 4x Laemmli buffer (10 µL of 240 mM Tris-HCl pH 6.8, 8% w/v SDS, 40% v/v glycerol, 5% v/v β-mercaptoethanol, 0.04% v/v/ bromophenol blue) and incubated at 95°C for 3 min. Samples were resolved by sodium dodecyl sulfate polyacrylamide gel electrophoresis (SDS-PAGE) on a 7.5% polyacrylamide gel (180 V, 70 min, 10 or 20 µL/lane). Gels were scanned using Cy2, Cy3 and Cy5 multichannel settings (532/28, 602/50 and 700/50 filters, respectively) on a ChemiDoc™ MP imager (Bio-Rad). Fluorescence intensity was quantified using Image Lab 6.0.1 (Bio-Rad) and corrected for protein loading as determined by Coomassie Brilliant Blue R-250 staining. Data was plotted using GraphPad Prism 8.0.

SRB proliferation assay

Assays were performed in 96-well plates (Greiner, Cellstar, 655180) by seeding (day 0), treatment (day 1) and subsequent incubation for 72 h. Cells were fixed, stained and staining was subsequently dissolved after which absorbance was measured. Each assay included the following controls: (i) a background control (to which no cells were added), (ii) t_0 controls (separate assay plate in which cells were fixed on

day 1, defined as 0% proliferation), (iii) nontreated controls (present in each assay plate, treated with vehicle and defined as 100% proliferation). Cells were treated with different concentrations of inhibitor, inhibitor + paclitaxel (4 nM) or paclitaxel (4 nM). All inhibitors were tested in two separate assays and all inhibitor concentrations were tested in triplicate per assay (N=2, n=3).

For each assay, U2OS cells from 10 cm dishes were seeded into 96-well plates (3,000 cells/well) and subsequently incubated overnight to allow for cell adherence. Vehicle, inhibitor and paclitaxel (stock solutions in DMSO) were diluted in complete medium to obtain 2x working solutions (1% DMSO). Cell medium was replaced by fresh complete medium (50 µL), treatment was started by addition of the 2x working solutions (50 µL) and plates were incubated at 37°C for 72 h. Cell medium was replaced by fresh serum free medium (100 µL) and cells were fixed by addition of 30 µL 50% (w/v) aq. trichloroacetic acid after which the plates were incubated at 4°C for 60 min. Wells were emptied by shaking the plates upside down after which wells were washed three times with demineralized water and air-dried overnight. To each well, 60 µL of SRB solution (0.4% (w/v) in 1% aq. acetic acid) was added and plates were incubated for 30 min. The excess SRB was removed and the wells were washed three times with 1% aq. acetic acid and air-dried overnight. Bound SRB was redissolved by addition of 150 µL 10 mM TRIS (free-base) and absorbance was measured at 540 nm on a CLARIOstar plate reader. Data was normalized between t_0 and nontreated controls and plotted using GraphPad Prism 8.0 using "Nonlinear regression (curve fit)" and "log(inhibitor) vs. normalized response – Variable slope" to determine pIC_{50} values.

Kinase selectivity profiling

Assays for determination of kinase selectivity were performed by Thermo Fisher Scientific's SelectScreen™ biochemical kinase profiling service. The complete list of tested kinases and inhibition profiles are shown in **Supplementary Table 6.1** (p. 210) and detailed assay procedures are described in SelectScreen Assay Conditions documents located at www.thermofisher.com/selectscreen under "SelectScreen kinase profiling Services" and then "Technology overview". The concentration of ATP was selected to be equal to the K_M, unless stated otherwise. Assays were performed with a compound concentration of 1 µM and kinases showing >50% inhibition were assayed again at a compound concentration of 100 nM. Data obtained from SelectScreen™ kinase assays were processed using KNIME Analytics Platform[30] (v.4.3.0). Inconsistent kinase naming was corrected. Seven kinases (BRAF, MAP2K1, MAP2K2, MAP2K6, JNK3, JNK1, JNK2) were present in two screening technologies and data for these kinases were therefore averaged resulting in 396 'unique' kinases (**Supplementary Table 6.1** (p. 210)). During screening of ROB433 (**15**), the assay to determine RPS6KB2 activity was not available and was therefore not measured (resulting in 395 'unique' kinases). The "genenames" database[31,32] was used to couple kinase names to Uniprot[33] IDs and Uniprot IDs were subsequently linked to kinase names accepted by KinMap[34] to generate **Supplementary Figure 6.3** (p. 209). Phosphatidylinositol kinases (16) and sphingosine kinases (2) were not visualized in **Supplementary Figure 6.3** (p. 209) and inhibition percentages of kinases that are tested with different combinations of subunits (for example AMPK) or kinases that are tested with different cyclins (for example CDKs) were averaged for the generation of **Supplementary Figure 6.3** (p. 209).

Oncolines™ profiling

Cell proliferation

Assays for determining the antiproliferative activity of ROB433 (**15**) were performed by the Oncolines™ profiling service. Detailed assay procedures are described at https://www.oncolines.com.[35] All cell lines have been licensed from the American Type Culture Collection (ATCC) Manassas, Virginia (US). Master and working cell banks (MCB and WCB) were prepared by subculturing in ATCC-recommended media and freezing according to ATCC recommended protocols (www.atcc.org). Cell line stocks for the assays were prepared from the WCB. The MCB, WCBs and assay stocks were prepared within respectively 3, 6 and 10 passages of the ATCC vial. Solid powder of ROB433 was weighed on a calibrated balance and dissolved in DMSO. At the day of the experiment, the compound stock (10 mM) was diluted in 3.16-fold steps in DMSO to obtain a 9-point dilution series which were all further diluted 31.6 times in 20 mM sterile HEPES buffer (pH 7.4). The final DMSO concentration during incubation was 0.4% in all wells. Cells were diluted in the corresponding ATCC recommended medium and dispensed in a 384-well plate,

depending on the cell line used, at a density of 100 - 6400 cells per well in 45 µL medium. For each cell line used, the optimal cell density was used. The margins of the plate were filled with PBS. Plated cells were incubated in a humidified atmosphere of 5% CO_2 at 37°C. After 24 h, 5 µL of compound (final concentrations were between 3.16 nM – 31.6 µM) was added and plates were incubated for 72 h. At t=end, 24 µL of ATPlite 1Step™ (PerkinElmer) solution was added to each well and plates were subsequently shaken for 2 min. After 10 min of incubation in the dark, the luminescence was recorded on an Envision multimode reader (PerkinElmer). Each compound concentration was tested in duplicate and half maximal inhibitory concentration (IC_{50}), half maximal growth inhibition concentration (GI_{50}) and half maximal lethal dose (LD_{50}) were determined as visualized by the graphs below.

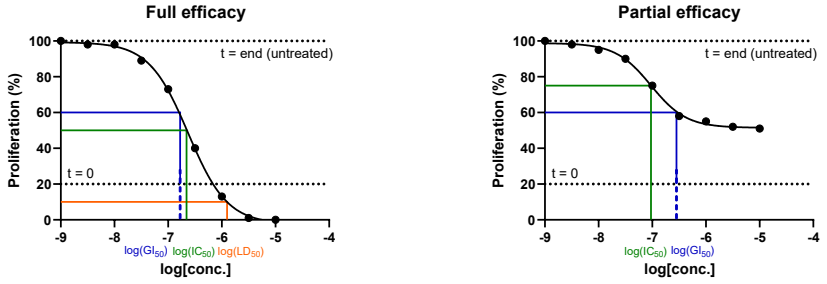

Controls cell proliferation

[t = 0 signal] – on a parallel plate, 45 µL cells were dispensed and incubated in a humidified atmosphere of 5% CO_2 at 37°C. After 24 h, 5 µL DMSO-containing HEPES buffer and 25 µL ATPlite 1Step™ solution were mixed, and luminescence measured after 10 min of incubation (=$luminescence_{t=0}$). [Reference compound] – the IC_{50} of reference compound doxorubicin is measured on a separate plate. The IC_{50} is trended. If the IC_{50} is out of specification (0.32 - 3.16 times deviating from historic average) the assay is invalidated. [Cell growth control] – the cellular doubling times of all cell lines are calculated from the t = 0 h and t = end growth signals of the untreated cells. If the doubling time is out of specification (0.5 – 2.0 times deviating from historical mean) the assay is invalidated. [t = end (untreated)] – for each cell line, the maximum luminescence was recorded after incubation until t = end without compound in the presence of 0.4% DMSO.

Drug sensitivity

The sensitivity distribution was analyzed across the tissue origin of the cell lines. The results are presented in a boxplot (**Figure 6.4A**). Tissue and disease types were annotated according to a cell line knowledge resource[36] and binned according to a widely used standardized classification[37]. Boxplots were generated for tissue types represented by at least two Oncolines™ cell lines. The large group of cell lines of colorectal origin was further divided according to a consensus classification based on gene expression.[38] These subtypes are biologically distinct and include CMS1 (MSI-immune), CMS2 (epithelial and canonical), CMS3 (epithelial and metabolic), and CMS4 (mesenchymal). Colorectal cell lines which could not significantly be assigned to a single subtype are annotated as 'No label'.

Cell genetics

The mutation status of cell lines was established from a combination of public and proprietary (NTRC) data. Based on public data (COSMIC Cancer Genome Project, version 80)[39,40], NTRC collected mutations, amplifications and deletions in established cancer driver genes that occur in Oncolines™.[41] For further validation, a selection of 23 cancer genes were sequenced by NTRC by targeted and full exome sequencing directly from the cell lines used in Oncolines™. As an extra filter, genetic changes were required to be observed with a preset frequency in patient tumor samples in COSMIC, depending on the type of genetic alteration. This discards sporadic, non-cancer-causing mutations. Cell lines were classified as having a 'wild type' or a 'mutated' genotype, where 'mutated' means: at least one allele changed by point mutation, insertion, deletion, amplification or copy number variation. Analysis was performed on genes that were mutated in at least three different Oncolines™ cell lines (98 genes in

total). A subset of the most commonly occurring and best known cancer genes (38 in total) was analyzed with type II Anova analysis in the statistical program R. For the genes which were significantly associated with drug response, genetic changes and drug sensitivities were visualized in waterfall plots.

Supplementary information

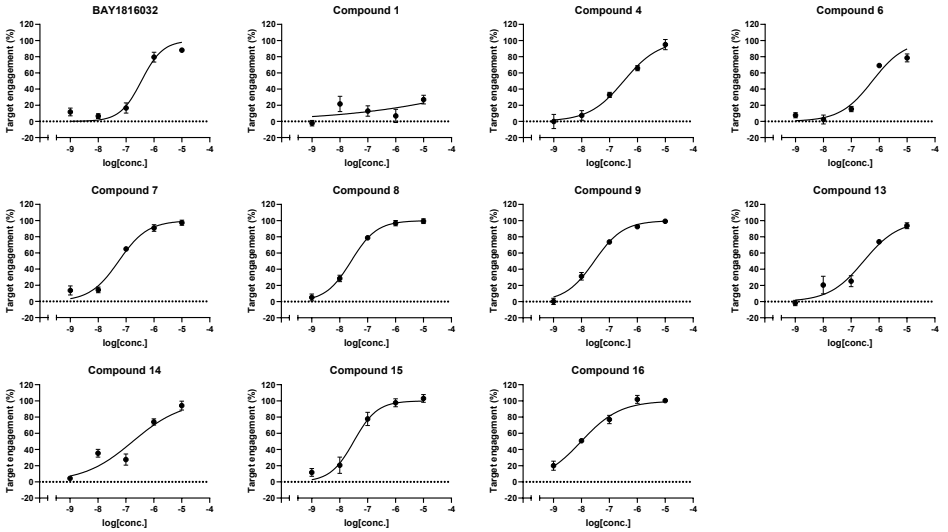

Supplementary Figure 6.1 | Dose-response curves of inhibitors on cellular BUB1 target engagement. All data were obtained using the target engagement assay as described in **Chapter 5**. U2OS-BUB1^{GFP_FLAG} cells were pre-incubated with different concentrations of indicated inhibitor (1 h, 37°C) followed by incubation with probe (1 µM, 1 h, 37°C). Cells were lysed, proteins labeled by probe were visualized by conjugation to a Cy5 fluorophore using click chemistry and samples were resolved by SDS-PAGE. In-gel fluorescence was measured, corrected for protein loading and normalized. Corresponding pTE_{50} values are reported in **Table 6.2**. Data represents mean ± SEM (N=3).

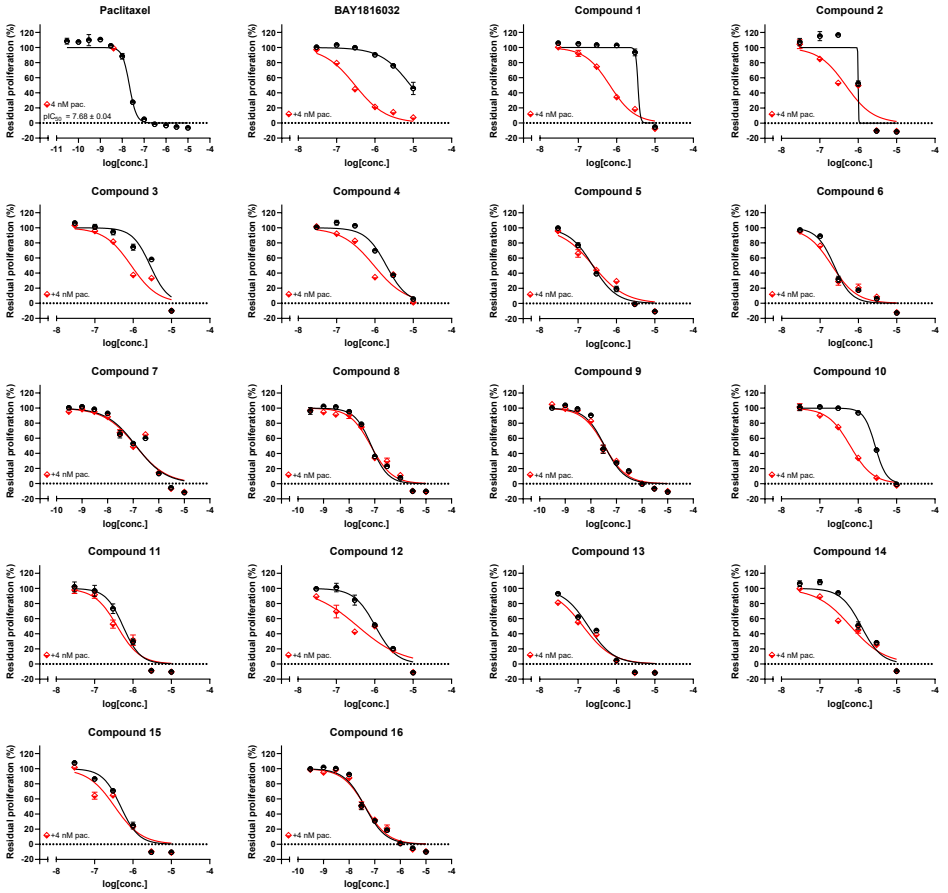

Supplementary Figure 6.2 | Dose-response curves of paclitaxel and BUB1 inhibitors on U2OS cell proliferation. All data were obtained using an SRB assay. Cells were treated with indicated inhibitor (black curves) or inhibitor + 4 nM paclitaxel (red curves) for 72 h after which cell proliferation was assessed. The effect of 4 nM of paclitaxel is indicated (red) in the graph of paclitaxel. Corresponding pIC_{50} values are reported in **Table 6.2**, except for paclitaxel which is reported in corresponding graph. Data represents mean ± SEM (at least N=2, n=3).

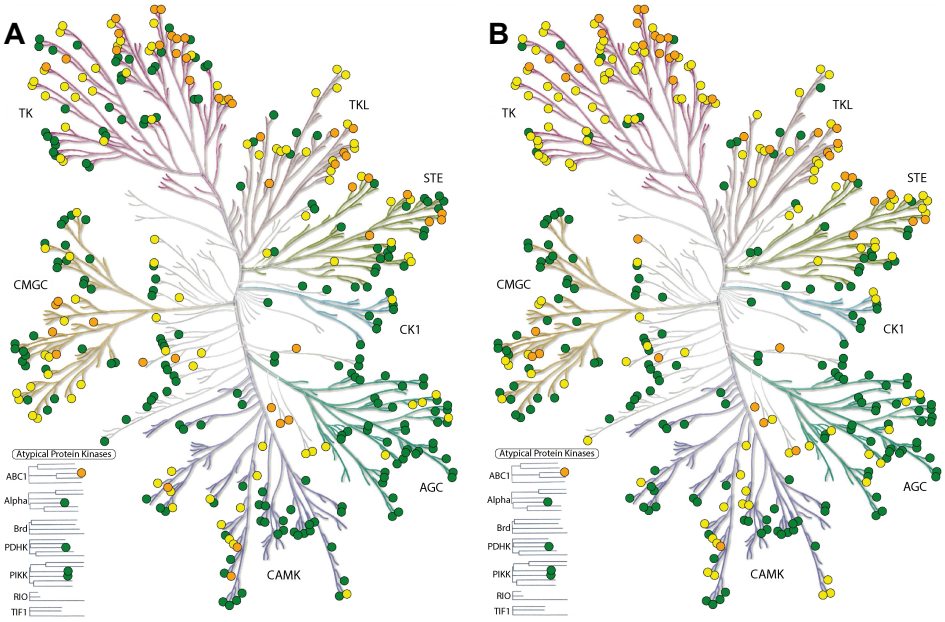

Supplementary Figure 6.3 | Representation of selectivity profiles of **(A)** ROB433 (**15**) and **(B)** ROB464 (**16**). Kinases not inhibited (≤50%) at a concentration of 1 μM are indicated in green, kinases inhibited (>50%) at 1 μM but not (≤50%) at 100 nM are indicated in yellow and kinases inhibited (>50%) at both 1 μM and 100 nM are indicated in orange. Images generated using KinMap[34], reproduced courtesy of Cell Signaling Technology, Inc. (www.cellsignal.com).

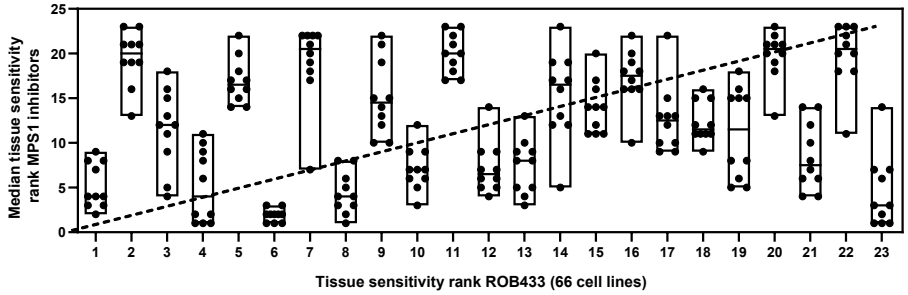

1. Uterus
2. Myeloid: chronic myeloid leukemia
3. Colorectal: CMS3
4. Lymphoid: non-hodgkin lymphoma
5. Kidney
6. Head and neck
7. Bone
8. Colorectal: CMS4
9. CNS: embryonal tumor
10. Lymphoid: lymphoblastic leukemia
11. Bladder
12. Colorectal: no label
13. CNS: diffuse glioma
14. Peripheral nervous system: neuroblastoma
15. Soft tissue
16. Pancreas
17. Cervix
18. Skin
19. Breast
20. Ovary
21. Lung: lung neuroendocrine tumor
22. Prostate
23. Lung: non-small cell lung cancer

Supplementary Figure 6.4 | Comparison of tissue sensitivity between ROB433 and MPS1 inhibitors. Previously, IC_{50} data from ten MPS1 inhibitors in 66 cell lines of the Oncolines™ profiling service was reported.[21] For each MPS1 inhibitor, IC_{50} values of cells originating from the same tissue, were averaged. Based on these averaged IC_{50} values, tissue sensitivity was ranked per compound (in which rank 1 is the most sensitive tissue). Per tissue, a box was generated in which each data point represents the rank of indicated tissue for one MPS1 inhibitor. The horizontal line inside each box represents the median rank among all ten MPS1 inhibitors within that tissue. Tissues were sorted (x-axis) based on the most sensitive tissue (=1) to ROB433 treatment among this panel of 66 cell lines. Of note, the tissue sensitivity rank of ROB433 varies slightly from that reported in **Figure 6.4A** since only data from 66 instead of 102 cell lines were included in this data set. The diagonal dashed line represents the same rank for both axes, median values close to this line therefore represents tissue with similar sensitivity to both ROB433 and MPS1 inhibitors. Median values distant to this line represent sensitivity to only either ROB433 or MPS1 inhibitors.

Supplementary Table 6.1 | Results of Thermo Fisher Scientific's SelectScreen™ biochemical kinase profiling service in a panel of 403 wild-type kinases (396 unique kinases, see Experimental section). Compound names (ROB433 (**15**) = 433 and ROB464 (**16**) = 464) and test concentrations are indicated in the column header. Only kinases that were inhibited (>50%) at a concentration of 1 µM were tested again at a concentration of 100 nM.

[µM]	433 1	433 0.1	464 1	464 0.1		[µM]	433 1	433 0.1	464 1	464 0.1		[µM]	433 1	433 0.1	464 1	464 0.1	
AAK1	92	66	58	12	•	CSNK1G1 (CK1 γ 1)	12		12			MAP2K2 (MEK2)	24		32		•
ABL1	61	38	93	28		CSNK1G2 (CK1 γ 2)	13		19			MAP2K4 (MEK4)	21		28		•
ABL2 (Arg)	68	37	88	33		CSNK1G3 (CK1 γ 3)	7		14			MAP2K5 (MEK5)	82	24	87	37	•
ACVR1 (ALK2)	94	52	94	57	•	CSNK2A1 (CK2 α 1)	2		4			MAP2K6 (MKK6)	11		30		•
ACVR1B (ALK4)	67	38	92	19		CSNK2A2 (CK2 α 2)	10		5			MAP3K10 (MLK2)	77	28	82	37	•
ACVR2A	72	19	79	30	•	DAPK1	48		-2			MAP3K11 (MLK3)	65	22	74	24	•
ACVR2B	98	55	91	42	•	DAPK2	70	37	-26		•	MAP3K14 (NIK)	56	11	11		•
ACVRL1 (ALK1)	92	59	88	56	•	DAPK3 (ZIPK)	32		7			MAP3K19 (YSK4)	88	52	98	35	
ADCK3	106	57	104	72	•	DCAMKL1 (DCLK1)	0		3			MAP3K2 (MEKK2)	95	50	97	89	•
ADRBK1 (GRK2)	4		3			DCAMKL2 (DCK2)	5		5			MAP3K3 (MEKK3)	101	69	91	99	•
ADRBK2 (GRK3)	-1		1			DDR1	89	66	96	45	•	MAP3K5 (ASK1)	-4		1		•
AKT1 (PKB α)	2		5			DDR2	77	30	90	33	•	MAP3K7/MAP3K7IP1 (TAK1-TAB1)	88	46	73	26	•
AKT2 (PKB β)	6		3			DMPK	50		74	27	•	MAP3K8 (COT)	11		10		‡
AKT3 (PKB γ)	3		9			DNAPK	3		8			MAP3K9 (MLK1)	79	34	94	20	
ALK	23		77	11		DYRK1A	21		1			MAP4K1 (HPK1)	89	43	91	52	•
AMPK (A1/B1/G1)	53	20	58	-1		DYRK1B	31		2			MAP4K2 (GCK)	40		87	12	
AMPK (A1/B1/G2)	79	33	71	30	•	DYRK2	54	13	-7		•	MAP4K3 (GLK)	68	43	74	45	•
AMPK (A1/B1/G3)	80	42	77	31	•	DYRK3	9		0			MAP4K4 (HGK)	88	52	102	48	
AMPK (A1/B2/G1)	79	35	66	21	•	DYRK4	0		-1			MAP4K5 (KHS1)	94	91	97	88	
AMPK (A1/B2/G2)	80	31	65	7		EEF2K	0		2			MAPK1 (ERK2)	6		5		
AMPK (A1/B2/G3)	71	24	69	12		EGFR (ErbB1)	32		92	26		MAPK10 (JNK3)	78	48	92	71	•
AMPK (A2/B1/G1)	68	18	80	9		EIF2AK2 (PKR)	54	7	82	54	•	MAPK11 (p38 β)	20		55	7	
AMPK (A2/B1/G2)	76	36	71	11		EPHA1	38		87	26		MAPK12 (p38 γ)	8		13		
AMPK (A2/B1/G3)	65	31	76	16		EPHA2	33		89	27		MAPK13 (p38 δ)	13		6		
AMPK (A2/B2/G1)	80	35	87	34	•	EPHA3	18		36		•	MAPK14 (p38 α)	35		90	19	‡
AMPK (A2/B2/G2)	83	42	87	42	•	EPHA4	37		90	17		MAPK14 (p38 α) Direct	31		91	23	
AMPK (A2/B2/G3)	88	35	67	14		EPHA5	39		89	20		MAPK15 (ERK7)	89	51	-1		•
ANKK1	49		54	24	•	EPHA6	92	68	92	95	•	MAPK3 (ERK1)	5		5		
AURKA (Aurora A)	98	84	100	77		EPHA7	85	41	95	75	•	MAPK7 (ERK5)	3		7		
AURKB (Aurora B)	94	71	97	43		EPHA8	52	17	90	32		MAPK8 (JNK1)	59	25	85	42	•
AURKC (Aurora C)	85	71	98	76		EPHB1	64	34	99	50		MAPK9 (JNK2)	86	52	91	76	•
AXL	72	24	89	20		EPHB2	57	8	98	33		MAPKAPK2	-6		-3		
BLK	48		88	21		EPHB3	-2		28			MAPKAPK3	-4		8		
BMPR1A (ALK3)	67	9	83	17	•	EPHB4	62	29	98	72		MAPKAPK5 (PRAK)	6		4		
BMPR1B (ALK6)	91	50	96	55	•	ERBB2 (HER2)	17		54	4		MARK1 (MARK)	23		15		
BMPR2	57	11	84	20	•	ERBB4 (HER4)	83	43	72	5		MARK2	18		12		
BMX	36		83	17		ERN1	76	15	58	16	•	MARK3	41		22		
BRAF	67	57	77	53	•	ERN2	28		19		•	MARK4	43		31		
BRSK1 (SAD1)	83	38	62	8		FER	39		97	23		MASTL	90	42	89	41	•
BRSK2	23		-12		•	FES (FPS)	32		80	8		MATK (HYL)	3		16		
BTK	25		84	11		FGFR1	92	47	100	62		MELK	68	21	89	20	
CAMK1 (CaMK1)	61	19	86	38	†	FGFR2	79	83	100	71		MERTK (cMER)	70	20	95	19	
CAMK1D (CaMKI δ)	16		58	8		FGFR3	87	58	96	64		MET (cMet)	33		84	5	
CAMK1G (CAMKI γ)	11		53	5		FGFR4	33		83	21		MINK1	98	70	102	66	
CAMK2A (CaMKII α)	9		0			FGR	83	43	97	42		MKNK1 (MNK1)	34		3		
CAMK2B (CaMKII β)	5		5			FLT1 (VEGFR1)	80	71	92	77		MKNK2 (MNK2)	38		-9		•
CAMK2D (CaMKII δ)	17		8			FLT3	94	84	96	58		MLCK2 (MLCK2)	78	26	55	9	•
CAMK2G (CaMKII γ)	5		5		•	FLT4 (VEGFR3)	94	83	99	67		MLK4	72	43	39		•
CAMK4 (CaMKIV)	-2		17			FRAP1 (mTOR)	0		-7			MST1R (RON)	45		60	8	
CAMKK1 (CAMKKA)	-1		34		•	FRK (PTK5)	24		63	8		MST4	-1		96	7	
CAMKK2 (CaMKK β)	20		4		•	FYN	67	18	90	29		MUSK	66	15	83	11	
CASK	0		4		•	FYN A	61	10	75	22	•	MYLK (MLCK)	66	16	44		•
CDC42BPA (MRCKA)	8		2			GAK	96	91	86	71	•	MYLK2 (skMLCK)	56	13	89	19	
CDC42BPB (MRCKB)	-1		2			GRK1	0		0		•	MYLK4	22		2		•
CDC42BPG (MRCKG)	22		39			GRK4	-3		-9			MYO3A (MYO3 α)	13		14		•
CDC7/DBF4	80	35	10		•	GRK5	0		0			MYO3B (MYO3 β)	45		35		•
CDK1/cyclin B	31		6			GRK6	4		-4			NEK1	4		63	-3	
CDK11 (Inactive)	4		1		•	GRK7	1		3			NEK2	10		48		
CDK11/cyclin C	4		-27		•	GSG2 (Haspin)	3		-3			NEK4	12		30		
CDK13/cyclin K	67	19	-1		•	GSK3A (GSK3 α)	99	95	78	13		NEK6	5		11		
CDK14 (PFTK1)/cyclin Y	53	7	8		•	GSK3B (GSK3 β)	101	96	71	3		NEK8	-8		-8		•
CDK16 (PCTK1)/cyclin Y	87	37	73	29	•	HCK	52	18	91	21		NEK9	9		26		
CDK17/cyclin Y	53	25	11			HIPK1 (Myak)	44		5			NIM1K	3		3		
CDK18/cyclin Y	35		3			HIPK2	63	17	9			NLK	103	69	102	84	•
CDK2/cyclin A	34		2			HIPK3 (YAK1)	49		0			NTRK1 (TRKA)	67	51	97	56	
CDK2/cyclin A1	56	17	1		•	HIPK4	50		-1			NTRK2 (TRKB)	66	28	97	39	
CDK2/cyclin E1	77	19	-13		•	HUNK	65	13	77	37	•	NTRK3 (TRKC)	91	53	101	89	
CDK2/cyclin O	77	40	34		•	ICK	77	31	2		•	NUAK1 (ARK5)	93	55	94	59	
CDK3/cyclin E1	51	7	-9		•	IGF1R	2		41			NUAK2	66	16	68	40	•
CDK4/cyclin D1	36		45		†	IKBKB (IKK β)	8		4			PAK1	15		17		
CDK4/cyclin D3	45		46		†	IKBKE (IKK epsilon)	27		78	8		PAK2 (PAK65)	5		13		
CDK5 (Inactive)	26		42		•	INSR	9		79	5		PAK3	-4		24		
CDK5/p25	56	21	6			INSRR (IRR)	28		86	17		PAK4	66	29	56	7	
CDK5/p35	68	23	12			IRAK1	42		24			PAK6	6		10		
CDK6/cyclin D1	55	15	61	6	†	IRAK3	64	31	-19		•	PAK7 (KIAA1264)	66	17	50		
CDK7/cyclin H/MNAT1	36		-1			IRAK4	10		9			PASK	2		2		
CDK8/cyclin C	15		-5		•	ITK	63	30	70	13		PDGFRA (PDGFR α)	71	35	96	67	
CDK9 (Inactive)	57	39	55	5	•	JAK1	54	15	79	11		PDGFRB (PDGFR β)	46		87	20	
CDK9/cyclin K	64	14	48		•	JAK2	95	83	100	81		PDK1	8		10		‡
CDK9/cyclin T1	85	29	62	11		JAK2 JH1 JH2	95	73	99	68		PDK1 Direct	20		58	1	
CDKL5	60	16	28			JAK3	90	56	93	22		PEAK1	54	30	93	11	
CHEK1 (CHK1)	27		20			KDR (VEGFR2)	99	100	101	76		PHKG1	6		6		
CHEK2 (CHK2)	9		7			KIT	16		43			PHKG2	4		5		
CHUK (IKK α)	34		13			KSR2	4		10			PI4K2A (PI4K2 α)	9		-3		†
CLK1	9		6			LATS2	33		63	19	•	PI4K2B (PI4K2 β)	8		3		†
CLK2	45		3			LCK	68	47	97	38		PI4KA (PI4K α)	6		3		†
CLK3	6		4			LIMK1	67	23	87	50	•	PI4KB (PI4K β)	7		-7		
CLK4	60	20	-8		•	LIMK2	77	23	91	46	•	PIK3C2A (PI3K-C2 α)	8		12		
CSF1R (FMS)	87	62	97	84		LRRK2	97	56	83	29		PIK3C2B (PI3K-C2 β)	15		82	15	†
CSK	25		60	6		LRRK2 FL	100	66	89	39		PIK3C2G (PI3K-C2 γ)	25		37		†
CSNK1A1 (CK1 α 1)	12		9			LTK (TYK1)	18		74	13		PIK3C3 (hVPS34)	6		3		
CSNK1A1L	4		8			LYN A	72	39	94	32		PIK3CA/PIK3R1 (p110 α/p85 α)	-8		0		
CSNK1D (CK1 δ)	35		85	16		LYN B	81	50	98	37		PIK3CA/PIK3R3 (p110 α/p55 γ)	7		5		†
CSNK1E (CK1 epsilon)	52	12	81	15		MAP2K1 (MEK1)	16		26		•	PIK3CB/PIK3R1 (p110 β/p85 α)	0		-10		

Supplementary Table 6.1 | (continued)

[μM]	433 1	433 0.1	464 1	464 0.1	
PIK3CB/PIK3R2 (p110 β/p85 β)	-5		-1		†
PIK3CD/PIK3R1 (p110 δ/p85 α)	14		3		
PIK3CG (p110 γ)	5		18		
PIM1	0		2		
PIM2	7		7		
PIM3	-1		7		
PIP4K2A	-6		14		†
PIP5K1A	79	37	44		†
PIP5K1B	89	55	54	12	†
PIP5K1C	95	50	55	6	†
PKMYT1	-6		14		•
PKN1 (PRK1)	4		34		
PKN2 (PRK2)	50		74	26	•
PLK1	4		1		
PLK2	4		20		
PLK3	-1		4		
PLK4	93	69	96	79	•
PRKACA (PKA)	6		46		
PRKACB (PRKAC β)	46		77	22	•
PRKACG (PRKAC γ)	61	19	82	39	•
PRKCA (PKC α)	33		15		
PRKCB1 (PKC β I)	-7		22		
PRKCB2 (PKC β II)	22		36		
PRKCD (PKC δ)	6		11		
PRKCE (PKC epsilon)	3		8		
PRKCG (PKC γ)	45		22		
PRKCH (PKC eta)	1		14		
PRKCI (PKC iota)	4		8		
PRKCN (PKD3)	31		68	12	
PRKCQ (PKC theta)	-4		14		
PRKCZ (PKC zeta)	-1		14		
PRKD1 (PKC mu)	40		66	13	
PRKD2 (PKD2)	44		70	13	
PRKG1	4		7		
PRKG2 (PKG2)	16		21		
PRKX	4		10		
PTK2 (FAK)	5		30		
PTK2B (FAK2)	39		97	49	
PTK6 (Brk)	75	14	94	43	
RET	99	97	99	94	
RIPK2	93	69	94	69	•
RIPK3	74	19	71	42	•
ROCK1	2		4		
ROCK2	2		10		
ROS1	84	32	95	25	
RPS6KA1 (RSK1)	52	8	47		
RPS6KA2 (RSK3)	67	22	51	5	
RPS6KA3 (RSK2)	36		44		
RPS6KA4 (MSK2)	20		26		
RPS6KA5 (MSK1)	16		27		
RPS6KA6 (RSK4)	65	22	66	8	
RPS6KB1 (p70S6K)	45		40		
RPS6KB2 (p70S6Kb)	N.D.	N.D.	5		
SBK1	4		14		
SGK (SGK1)	58	18	20		
SGK2	28		24		
SGKL (SGK3)	3		2		
SIK1	31		60	10	•
SIK3	25		33		•
SLK	94	64	98	87	•
SNF1LK2	81	52	87	32	
SPHK1	-3		4		
SPHK2	-5		-19		†
SRC	53	37	94	23	
SRMS (Srm)	10		45		
SRPK1	2		4		
SRPK2	2		3		
STK16 (PKL12)	90	23	61	12	•
STK17A (DRAK1)	87	23	6		•
STK17B (DRAK2)	66	79	-7		•
STK22B (TSSK2)	2		3		
STK22D (TSSK1)	84	30	9		
STK23 (MSSK1)	0		-1		
STK24 (MST3)	9		78	-3	
STK25 (YSK1)	13		55	0	
STK3 (MST2)	15		34		
STK32B (YANK2)	86	44	98	81	•
STK32C (YANK3)	54	9	87	38	•
STK33	59	11	55	10	•
STK38 (NDR)	36		29		•
STK38L (NDR2)	39		47		•
STK39 (STLK3)	24		50		•
STK4 (MST1)	18		59	6	
SYK	77	33	73	7	
TAOK1	86	44	77	49	•
TAOK2 (TAO1)	41		96	23	
TAOK3 (JIK)	33		56	19	•
TBK1	58	15	47		
TEC	8		-1		•
TEK (Tie2)	98	80	100	85	
TESK1	84	50	91	62	•
TESK2	26		44		•
TGFBR1 (ALK5)	99	93	99	94	•
TGFBR2	71	48	79	13	•
TLK1	-2		-8		•
TLK2	40		-2		•
TNIK	96	64	97	92	•
TNK1	49		82	16	
TNK2 (ACK)	22		60	10	•
TTK	33		10		•
TXK	37		84	11	
TYK2	97	60	97	31	
TYRO3 (RSE)	45		75	7	
ULK1	7		-2		•
ULK2	16		6		•
ULK3	59	22	28		•
VRK2	-1		19		•
WEE1	35		47		•
WNK1	9		10		•
WNK2	77	21	93	50	•
WNK3	50		80	20	•
YES1	98	85	100	91	
ZAK	12		9		•
ZAP70	7		9		

• LanthaScreen technology, no ATP; † = 10 μM ATP; ‡ = 100 μM ATP; N.D. = not determined.

Supplementary Table 6.2 | Results of the Oncolines™ profiling service in a panel of 102 cancer cell lines originating from different tissues. ROB433 (**15**) was tested at nine concentrations. Dose-response curves that were biphasic are indicated (•). Max eff.: maximal effect (%), pIC_{50}: half maximal inhibitory concentration, pGI_{50}: half maximal growth inhibitory concentration, pLD_{50}: half maximal lethal dose, all as –log(molar concentration) and determined as described in the Experimental section.

Cell line	ATCC ref	Tissue	Disease	pIC_{50}	Max eff. (%)	pGI_{50}	pLD_{50}
5637	HTB-9	Bladder/Urinary Tract	Bladder carcinoma	6.00	98	6.07	5.76
769-P	CRL-1933	Kidney	Renal cell carcinoma	6.26	100	6.24	5.40
786-O	CRL-1932	Kidney	Renal cell carcinoma	5.71	100	5.70	5.19
A-172	CRL-1620	CNS/Brain	Glioblastoma	5.81	100	5.89	5.34
A-204	HTB-82	Soft tissue	Embryonal rhabdomyosarcoma	5.91	100	5.99	5.37
A375	CRL-1619	Skin	Amelanotic melanoma	6.06	100	6.07	4.92
A388	CRL-7905	Skin	Squamous cell carcinoma	5.75	100	5.76	5.58
A-427	HTB-53	Lung	Lung adenocarcinoma	5.95	100	5.97	5.69
A-498	HTB-44	Kidney	Renal cell carcinoma	6.09	100	6.13	5.47
A-549	CCL-185	Lung	Lung adenocarcinoma	5.53	100	5.59	4.92
A-704	HTB-45	Kidney	Renal cell carcinoma	6.00	100	6.13	5.82
ACHN	CRL-1611	Kidney	Papillary renal cell carcinoma	6.03	100	6.05	5.59
AN3 CA	HTB-111	Uterus	Endometrial adenocarcinoma	7.28	38	<6.50	<5.50•
AsPC-1	CRL-1682	Pancreas	Pancreatic ductal adenocarcinoma	5.72	100	5.77	5.60
AU-565	CRL-2351	Breast	Breast adenocarcinoma	5.39	99	5.46	5.24
BT-20	HTB-19	Breast	Invasive ductal carcinoma	5.75	100	5.86	5.51
BT-549	HTB-122	Breast	Invasive ductal carcinoma	5.80	100	5.87	5.36
BxPC-3	CRL-1687	Pancreas	Pancreatic ductal adenocarcinoma	5.78	100	5.80	5.49
C-33 A	HTB-31	Cervix	Cervical squamous cell carcinoma	5.87	100	5.91	5.70
CAL 27	CRL-2095	Head and Neck	Tongue squamous cell carcinoma	6.19	100	6.19	5.71
CCF-STTG1	CRL-1718	CNS/Brain	Astrocytoma	5.75	98	5.78	5.62
CCRF-CEM	CCL-119	Lymphoid	Childhood T acute lymphoblastic leukemia	6.52	98	6.54	6.29
COLO 205	CCL-222	Bowel	Colon adenocarcinoma	5.94	100	5.96	5.57
COLO 829	CRL-1974	Skin	Cutaneous melanoma	5.39	100	5.43	5.24
Daoy	HTB-186	CNS/Brain	Medulloblastoma	5.89	100	5.94	5.55
DB	CRL-2289	Lymphoid	Diffuse large B-cell lymphoma	6.51	100	6.57	6.29
DLD-1	CCL-221	Bowel	Colon adenocarcinoma	5.50	100	5.52	4.94
DoTc2 4510	CRL-7920	Cervix	Cervical carcinoma	5.67	100	5.72	5.25
DU 145	HTB-81	Prostate	Prostate carcinoma	5.92	99	5.92	5.45
DU4475	HTB-123	Breast	Breast carcinoma	5.91	100	5.97	5.70
ES-2	CRL-1978	Ovary/Fallopian Tube	Ovarian clear cell adenocarcinoma	5.82	100	5.83	5.52
FaDu	HTB-43	Head and Neck	Hypopharyngeal squamous cell carcinoma	5.88	99	5.91	5.42
G-361	CRL-1424	Skin	Melanoma	5.74	100	5.77	5.59
HCT 116	CCL-247	Bowel	Colon carcinoma	6.27	98	6.22	5.31
HCT-15	CCL-225	Bowel	Colon adenocarcinoma	5.85	100	5.85	5.05
HL-60	CCL-240	Myeloid	Adult acute myeloid leukemia	5.76	100	5.79	5.63
Hs 578T	HTB-126	Breast	Invasive ductal carcinoma	6.23	100	6.30	5.72
Hs 746T	HTB-135	Esophagus/Stomach	Gastric adenocarcinoma	5.86	100	5.93	5.52
Hs 766T	HTB-134	Pancreas	Pancreatic adenocarcinoma	5.70	99	5.75	5.55
HT	CRL-2260	Lymphoid	Diffuse large B-cell lymphoma	5.82	100	5.86	5.68
HT-1080	CCL-121	Soft Tissue	Fibrosarcoma	5.97	100	5.90	5.45
HuTu 80	HTB-40	Bowel	Duodenal adenocarcinoma	6.66	100	6.65	5.53
J82	HTB-1	Bladder/Urinary Tract	Bladder carcinoma	5.87	99	5.95	5.63
JAR	HTB-144	Uterus	Gestational choriocarcinoma	6.22	100	6.25	5.48
Jurkat E6.1	TIB-152	Lymphoid	Childhood T acute lymphoblastic leukemia	5.92	100	5.96	5.63
K-562	CCL-243	Myeloid	Chronic myelogenous leukemia	6.23	100	6.26	5.50
KATO III	HTB-103	Esophagus/Stomach	Signet ring cell gastric adenocarcinoma	7.00	70	6.98	<6.00•
KG-1	CCL-246	Myeloid	Adult acute myeloid leukemia	6.97	68	7.00	<6.00•
KLE	CRL-1622	Uterus	Endometrial adenocarcinoma	5.59	100	5.75	5.42
KU812	CRL-2099	Myeloid	Chronic myelogenous leukemia	5.96	100	6.00	5.85
LNCaP FGC	CRL-1740	Prostate	Prostate carcinoma	5.42	100	5.48	5.32
LoVo	CCL-229	Bowel	Colon adenocarcinoma	5.80	100	5.91	5.28
LS 174T	CL-188	Bowel	Colon adenocarcinoma	6.15	100	6.14	5.43
LS411N	CRL-2159	Bowel	Cecum adenocarcinoma	5.91	100	5.95	5.44
MCF7	HTB-22	Breast	Invasive ductal carcinoma	5.41	100	5.47	5.32
MeWo	HTB-65	Skin	Melanoma	5.72	100	5.74	5.56
MG-63	CRL-1427	Bone	Osteosarcoma	5.93	100	5.95	5.74
MIA PaCa-2	CRL-1420	Pancreas	Pancreatic ductal adenocarcinoma	5.88	100	5.91	5.50
MOLT-4	CRL-1582	Lymphoid	Adult T acute lymphoblastic leukemia	5.85	100	5.91	5.66
NCCIT	CRL-2073	Testis	Testicular embryonal carcinoma	5.95	100	5.92	5.32
NCI-H460	HTB-177	Lung	Large cell lung carcinoma	5.43	100	5.43	4.94
NCI-H661	HTB-183	Lung	Large cell lung carcinoma	5.51	100	5.73	5.27
NCI-H82	HTB-175	Lung	Small cell lung carcinoma	5.89	100	5.92	5.61
OVCAR-3	HTB-161	Ovary/Fallopian Tube	High grade ovarian serous adenocarcinoma	5.62	100	5.79	5.39
PA-1	CRL-1572	Ovary/Fallopian Tube	Ovarian mixed germ cell tumor	5.85	100	5.88	5.66
PC-3	CRL-1435	Prostate	Prostate carcinoma	5.60	100	5.72	5.14
PFSK-1	CRL-2060	CNS/Brain	Primitive neuroectodermal tumor	5.63	99	5.64	5.46
RD	CCL-136	Soft tissue	Embryonal rhabdomyosarcoma	6.19	100	6.30	5.56
RKO	CRL-2577	Bowel	Colon carcinoma	5.82	100	5.84	5.53
RL	CRL-2261	Lymphoid	Diffuse large B-cell lymphoma	6.00	100	6.04	5.68
RL95-2	CRL-1671	Uterus	Endometrial adenosquamous carcinoma	5.69	100	5.74	5.58
RPMI-7951	HTB-66	Skin	Melanoma	6.13	100	6.19	5.58
RS4-11	CRL-1873	Lymphoid	Adult B acute lymphoblastic leukemia	6.34	100	6.36	5.89
RT4	HTB-2	Bladder/Urinary Tract	Bladder carcinoma	5.87	100	6.07	5.41
SHP-77	CRL-2195	Lung	Small cell lung carcinoma	5.45	96	5.54	5.21
SJCRH30	CRL-2061	Soft tissue	Alveolar rhabdomyosarcoma	5.80	100	5.85	5.65
SK-N-AS	CRL-2137	Peripheral Nervous System	Neuroblastoma	5.72	100	5.78	5.45

Supplementary Table 6.2 | (continued)

Cell line	ATCC ref	Tissue	Disease	pIC_{50}	Max eff. (%)	pGI_{50}	pLD_{50}
SK-N-FI	CRL-2142	Peripheral Nervous System	Neuroblastoma	5.93	99	6.06	5.62
SNU-5	CRL-5973	Esophagus/Stomach	Gastric carcinoma	5.98	100	6.14	5.42
SNU-C2B	CCL-250	Bowel	Cecum adenocarcinoma	5.78	100	5.83	5.63
SR	CRL-2262	Lymphoid	Anaplastic large cell lymphoma	6.03	99	6.05	5.73
SU-DHL-1	CRL-2955	Lymphoid	Anaplastic large cell lymphoma	5.87	100	5.88	5.58
SU-DHL-6	CRL-2959	Lymphoid	Diffuse large B-cell lymphoma	6.17	99	6.31	5.77
SUP-T1	ACC140	Lymphoid	Childhood T lymphoblastic lymphoma	5.69	100	5.71	5.52
SW48	CCL-231	Bowel	Colon adenocarcinoma	6.51	87	6.52	<5.50•
SW480	CCL-228	Bowel	Colon adenocarcinoma	5.60	100	5.61	5.41
SW620	CCL-227	Bowel	Colon adenocarcinoma	6.09	100	6.11	5.84
SW626	HTB-78	Bowel	Colon adenocarcinoma	5.55	100	5.58	5.29
SW837	CCL-235	Bowel	Rectal adenocarcinoma	5.55	99	5.66	5.07
SW872	HTB-92	Soft tissue	Liposarcoma	5.67	100	5.70	5.02
SW900	HTB-59	Lung	Squamous cell lung carcinoma	5.78	99	5.78	5.24
SW948	CCL-237	Bowel	Colon adenocarcinoma	6.04	99	6.08	5.68
SW982	HTB-93	Soft Tissue	Biphasic synovial sarcoma	6.16	99	6.21	5.55
T24	HTB-4	Bladder/Urinary Tract	Bladder carcinoma	5.87	100	5.86	5.64
T98G	CRL-1690	CNS/Brain	Glioblastoma	6.15	100	6.18	5.56
TCCSUP	HTB-5	Bladder/Urinary Tract	Bladder carcinoma	5.58	99	5.59	5.43
THP-1	TIB-202	Myeloid	Childhood acute monocytic leukemia	5.22	99	5.25	5.10
TT	CRL-1803	Thyroid	Hereditary thyroid gland medullary carcinoma	5.31	100	5.48	5.23
U-118 MG	HTB-15	CNS/Brain	Astrocytoma	5.80	100	5.83	5.60
U-2 OS	HTB-96	Bone	Osteosarcoma	5.93	100	5.99	5.65
U-87 MG	HTB-14	CNS/Brain	Glioblastoma	5.82	99	5.83	5.49
VA-ES-BJ	CRL-2138	Soft Tissue	Epithelioid sarcoma	5.57	100	5.59	5.42

References

1. Walczak, C. E., Cai, S. & Khodjakov, A. Mechanisms of chromosome behaviour during mitosis. *Nat. Rev. Mol. Cell Biol.* **11**, 91–102 (2010).
2. Kops, G. J. P. L., Weaver, B. A. A. & Cleveland, D. W. On the road to cancer: aneuploidy and the mitotic checkpoint. *Nat. Rev. Cancer* **5**, 773–785 (2005).
3. Musacchio, A. & Salmon, E. D. The spindle-assembly checkpoint in space and time. *Nat. Rev. Mol. Cell Biol.* **8**, 379–393 (2007).
4. Dominguez-Brauer, C., Thu, K. L., Mason, J. M., Blaser, H., Bray, M. R. & Mak, T. W. Targeting Mitosis in Cancer: Emerging Strategies. *Mol. Cell* **60**, 524–536 (2015).
5. Gallego-Jara, J., Lozano-Terol, G., Sola-Martínez, R. A., Cánovas-Díaz, M. & de Diego Puente, T. A Compressive Review about Taxol®: History and Future Challenges. *Molecules* **25**, 5986 (2020).
6. Weaver, B. A. How Taxol/paclitaxel kills cancer cells. *Mol. Biol. Cell* **25**, 2677–2681 (2014).
7. Markman, M. Managing taxane toxicities. *Support. Care Cancer* **11**, 144–147 (2003).
8. Janssen, A., Kops, G. J. P. L. & Medema, R. H. Elevating the frequency of chromosome mis-segregation as a strategy to kill tumor cells. *Proc. Natl. Acad. Sci.* **106**, 19108–19113 (2009).
9. Maia, A. R. R., de Man, J., Boon, U., Janssen, A., Song, J.-Y., Omerzu, M., Sterrenburg, J. G., Prinsen, M. B. W., Willemsen-Seegers, N., de Roos, J. A. D. M., van Doornmalen, A. M., Uitdehaag, J. C. M., Kops, G. J. P. L., Jonkers, J., Buijsman, R. C., Zaman, G. J. R. & Medema, R. H. Inhibition of the spindle assembly checkpoint kinase TTK enhances the efficacy of docetaxel in a triple-negative breast cancer model. *Ann. Oncol.* **26**, 2180–2192 (2015).
10. Siemeister, G., Mengel, A., Fernández-Montalván, A. E., Bone, W., Schröder, J., Zitzmann-Kolbe, S., Briem, H., Prechtl, S., Holton, S. J., Mönning, U., von Ahsen, O., Johanssen, S., Cleve, A., Pütter, V., Hitchcock, M., von Nussbaum, F., Brands, M., Ziegelbauer, K. & Mumberg, D. Inhibition of BUB1 Kinase by BAY 1816032 Sensitizes Tumor Cells toward Taxanes, ATR, and PARP Inhibitors *In Vitro* and *In Vivo*. *Clin. Cancer Res.* **25**, 1404–1414 (2019).
11. Zhang, G., Kruse, T., Guasch Boldú, C., Garvanska, D. H., Coscia, F., Mann, M., Barisic, M. & Nilsson, J. Efficient mitotic checkpoint signaling depends on integrated activities of Bub1 and the RZZ complex. *EMBO J.* **38**, (2019).
12. Lovly, C. M. & Shaw, A. T. Molecular Pathways: Resistance to Kinase Inhibitors and Implications for Therapeutic Strategies. *Clin. Cancer Res.* **20**, 2249–2256 (2014).
13. Hann, M. M. & Simpson, G. L. Intracellular drug concentration and disposition – The missing link? *Methods* **68**, 283–285 (2014).
14. Vichai, V. & Kirtikara, K. Sulforhodamine B colorimetric assay for cytotoxicity screening. *Nat. Protoc.* **1**, 1112–1116 (2006).
15. Skehan, P., Storeng, R., Scudiero, D., Monks, A., McMahon, J., Vistica, D., Warren, J. T., Bokesch, H., Kenney, S. & Boyd, M. R. New Colorimetric Cytotoxicity Assay for Anticancer-Drug Screening. *JNCI J. Natl. Cancer Inst.* **82**, 1107–1112 (1990).
16. Dragon, S., Hille, R., Götz, R. & Baumann, R. Adenosine 3′:5′-Cyclic Monophosphate (cAMP)-Inducible Pyrimidine 5′-Nucleotidase and Pyrimidine Nucleotide Metabolism of Chick Embryonic Erythrocytes. *Blood* **91**, 3052–3058 (1998).
17. Gribble, F. M., Loussouarn, G., Tucker, S. J., Zhao, C., Nichols, C. G. & Ashcroft, F. M. A Novel Method for Measurement of Submembrane ATP Concentration. *J. Biol. Chem.* **275**, 30046–30049 (2000).
18. Pathak, D., Shields, L. Y., Mendelsohn, B. A., Haddad, D., Lin, W., Gerencser, A. A., Kim, H., Brand, M. D., Edwards, R. H. & Nakamura, K. The Role of Mitochondrially Derived ATP in Synaptic Vesicle Recycling. *J. Biol. Chem.* **290**, 22325–22336 (2015).
19. Rangaraju, V., Calloway, N. & Ryan, T. A. Activity-Driven Local ATP Synthesis Is Required for Synaptic Function. *Cell* **156**, 825–835 (2014).
20. Uitdehaag, J. C. M., Kooijman, J. J., de Roos, J. A. D. M., Prinsen, M. B. W., Dylus, J., Willemsen-Seegers, N., Kawase, Y., Sawa, M., de Man, J., van Gerwen, S. J. C., Buijsman, R. C. & Zaman, G. J. R. Combined Cellular and Biochemical Profiling to Identify Predictive Drug Response Biomarkers for Kinase Inhibitors Approved for Clinical Use between 2013 and 2017. *Mol. Cancer Ther.* **18**, 470–481 (2019).
21. Zaman, G. J. R., de Roos, J. A. D. M., Libouban, M. A. A., Prinsen, M. B. W., de Man, J., Buijsman, R. C. & Uitdehaag, J. C. M. TTK Inhibitors as a Targeted Therapy for CTNNB1 (β-catenin) Mutant Cancers. *Mol. Cancer Ther.* **16**, 2609–2617 (2017).
22. Jemaà, M., Galluzzi, L., Kepp, O., Senovilla, L., Brands, M., Boemer, U., Koppitz, M., Lienau, P., Prechtl, S., Schulze, V., Siemeister, G., Wengner, A. M., Mumberg, D., Ziegelbauer, K., Abrieu, A., Castedo, M., Vitale, I. & Kroemer, G. Characterization of novel MPS1 inhibitors with preclinical anticancer activity. *Cell Death Differ.* **20**, 1532–1545 (2013).
23. Kusakabe, K., Ide, N., Daigo, Y., Itoh, T., Higashino, K., Okano, Y., Tadano, G., Tachibana, Y., Sato, Y., Inoue, M., Wada, T., Iguchi, M., Kanazawa, T., Ishioka, Y., Dohi, K., Tagashira, S., Kido, Y., Sakamoto, S., Yasuo, K., Maeda, M., Yamamoto, T., Higaki, M., Endoh, T., Ueda, K., Shiota, T., Murai, H. & Nakamura, Y. Diaminopyridine-Based Potent and Selective Mps1 Kinase Inhibitors Binding to an Unusual Flipped-Peptide Conformation. *ACS Med. Chem. Lett.* **3**, 560–564 (2012).

24. Anastas, J. N. & Moon, R. T. WNT signalling pathways as therapeutic targets in cancer. *Nat. Rev. Cancer* **13**, 11–26 (2013).
25. Etemadmoghadam, D., deFazio, A., Beroukhim, R., Mermel, C., George, J., Getz, G., Tothill, R., Okamoto, A., Raeder, M. B., AOCS Study Group, Harnett, P., Lade, S., Akslen, L. A., Tinker, A. V., Locandro, B., Alsop, K., Chiew, Y.-E., Traficante, N., Fereday, S., Johnson, D., Fox, S., Sellers, W., Urashima, M., Salvesen, H. B., Meyerson, M. & Bowtell, D. Integrated Genome-Wide DNA Copy Number and Expression Analysis Identifies Distinct Mechanisms of Primary Chemoresistance in Ovarian Carcinomas. *Clin. Cancer Res.* **15**, 1417–1427 (2009).
26. Patch, A.-M., Christie, E. L., Etemadmoghadam, D., Garsed, D. W., George, J., Fereday, S., Nones, K., Cowin, P., Alsop, K., Bailey, P. J., Kassahn, K. S., Newell, F., Quinn, M. C. J., Kazakoff, S., Quek, K., Wilhelm-Benartzi, C., Curry, E., Leong, H. S., Hamilton, A., Mileshkin, L., Au-Yeung, G., Kennedy, C., Hung, J., Chiew, Y.-E., Harnett, P., Friedlander, M., Quinn, M., Pyman, J., Cordner, S., O'Brien, P., Leditschke, J., Young, G., Strachan, K., Waring, P., Azar, W., Mitchell, C., Traficante, N., Hendley, J., Thorne, H., Shackleton, M., Miller, D. K., Arnau, G. M., Tothill, R. W., Holloway, T. P., Semple, T., Harliwong, I., Nourse, C., Nourbakhsh, E., Manning, S., Idrisoglu, S., Bruxner, T. J. C., Christ, A. N., Poudel, B., Holmes, O., Anderson, M., Leonard, C., Lonie, A., Hall, N., Wood, S., Taylor, D. F., Xu, Q., Fink, J. L., Waddell, N., Drapkin, R., Stronach, E., Gabra, H., Brown, R., Jewell, A., Nagaraj, S. H., Markham, E., Wilson, P. J., Ellul, J., McNally, O., Doyle, M. A., Vedururu, R., Stewart, C., Lengyel, E., Pearson, J. V., Waddell, N., deFazio, A., Grimmond, S. M. & Bowtell, D. D. L. Whole–genome characterization of chemoresistant ovarian cancer. *Nature* **521**, 489–494 (2015).
27. Rose, M., Burgess, J. T., O'Byrne, K., Richard, D. J. & Bolderson, E. PARP Inhibitors: Clinical Relevance, Mechanisms of Action and Tumor Resistance. *Front. Cell Dev. Biol.* **8**, 564601 (2020).
28. Etemadmoghadam, D., Weir, B. A., Au-Yeung, G., Alsop, K., Mitchell, G., George, J., Australian Ovarian Cancer Study Group, Davis, S., D'Andrea, A. D., Simpson, K., Hahn, W. C. & Bowtell, D. D. L. Synthetic lethality between CCNE1 amplification and loss of BRCA1. *Proc. Natl. Acad. Sci.* **110**, 19489–19494 (2013).
29. Yang, C., Wang, H., Xu, Y., Brinkman, K. L., Ishiyama, H., Wong, S. T. C. & Xu, B. The kinetochore protein Bub1 participates in the DNA damage response. *DNA Repair* **11**, 185–191 (2012).
30. Berthold, M. R., Cebron, N., Dill, F., Gabriel, T. R., Kötter, T., Meinl, T., Ohl, P., Thiel, K. & Wiswedel, B. KNIME - the Konstanz Information Miner: Version 2.0 and Beyond. *SIGKDD Explor Newsl* **11**, 26–31 (2009).
31. HGNC Database, HUGO Gene Nomenclature Committee (HGNC), European Molecular Biology Laboratory, European Bioinformatics Institute (EMBL-EBI), Wellcome Genome Campus, Hinxton, Cambridge CB10 1SD, United Kingdom www.genenames.org. *(accessed in April 2021)* https://www.accessdata.fda.gov/drugsatfda_docs/nda/2013/205552Orig1s000TOC.cfm.
32. Tweedie, S., Braschi, B., Gray, K., Jones, T. E. M., Seal, R. L., Yates, B. & Bruford, E. A. Genenames.org: the HGNC and VGNC resources in 2021. *Nucleic Acids Res.* **49**, D939–D946 (2021).
33. The UniProt Consortium. UniProt: the universal protein knowledgebase in 2021. *Nucleic Acids Res.* **49**, D480–D489 (2021).
34. Eid, S., Turk, S., Volkamer, A., Rippmann, F. & Fulle, S. KinMap: a web-based tool for interactive navigation through human kinome data. *BMC Bioinformatics* **18**, 16 (2017).
35. Uitdehaag, J. C. M., de Roos, J. A. D. M., van Doornmalen, A. M., Prinsen, M. B. W., de Man, J., Tanizawa, Y., Kawase, Y., Yoshino, K., Buijsman, R. C. & Zaman, G. J. R. Comparison of the Cancer Gene Targeting and Biochemical Selectivities of All Targeted Kinase Inhibitors Approved for Clinical Use. *PLoS ONE* **9**, e92146 (2014).
36. Bairoch, A. The Cellosaurus, a Cell-Line Knowledge Resource. *J. Biomol. Tech. JBT* **29**, 25–38 (2018).
37. Kundra, R., Zhang, H., Sheridan, R., Sirintrapun, S. J., Wang, A., Ochoa, A., Wilson, M., Gross, B., Sun, Y., Madupuri, R., Satravada, B. A., Reales, D., Vakiani, E., Al-Ahmadie, H. A., Dogan, A., Arcila, M., Zehir, A., Maron, S., Berger, M. F., Viaplana, C., Janeway, K., Ducar, M., Sholl, L., Dogan, S., Bedard, P., Surrey, L. F., Sanchez, I. H., Syed, A., Rema, A. B., Chakravarty, D., Suehnholz, S., Nissan, M., Iyer, G. V., Murali, R., Bouvier, N., Soslow, R. A., Hyman, D., Younes, A., Intlekofer, A., Harding, J. J., Carvajal, R. D., Sabbatini, P. J., Abou-Alfa, G. K., Morris, L., Janjigian, Y. Y., Gallagher, M. M., Soumerai, T. A., Mellinghoff, I. K., Hakimi, A. A., Fury, M., Huse, J. T., Bagrodia, A., Hameed, M., Thomas, S., Gardos, S., Cerami, E., Mazor, T., Kumari, P., Raman, P., Shivdasani, P., MacFarland, S., Newman, S., Waanders, A., Gao, J., Solit, D. & Schultz, N. OncoTree: A Cancer Classification System for Precision Oncology. *JCO Clin. Cancer Inform.* 221–230 (2021).
38. Sveen, A., Bruun, J., Eide, P. W., Eilertsen, I. A., Ramirez, L., Murumägi, A., Arjama, M., Danielsen, S. A., Kryeziu, K., Elez, E., Tabernero, J., Guinney, J., Palmer, H. G., Nesbakken, A., Kallioniemi, O., Dienstmann, R. & Lothe, R. A. Colorectal Cancer Consensus Molecular Subtypes Translated to Preclinical Models Uncover Potentially Targetable Cancer Cell Dependencies. *Clin. Cancer Res.* **24**, 794–806 (2018).
39. Tate, J. G., Bamford, S., Jubb, H. C., Sondka, Z., Beare, D. M., Bindal, N., Boutselakis, H., Cole, C. G., Creatore, C., Dawson, E., Fish, P., Harsha, B., Hathaway, C., Jupe, S. C., Kok, C. Y., Noble, K., Ponting, L., Ramshaw, C. C., Rye, C. E., Speedy, H. E., Stefancsik, R., Thompson, S. L., Wang, S., Ward, S., Campbell, P. J. & Forbes, S. A. COSMIC: the Catalogue Of Somatic Mutations In Cancer. *Nucleic Acids Res.* **47**, D941–D947 (2019).
40. Garnett, M. J., Edelman, E. J., Heidorn, S. J., Greenman, C. D., Dastur, A., Lau, K. W., Greninger, P., Thompson, I. R., Luo, X., Soares, J., Liu, Q., Iorio, F., Surdez, D., Chen, L., Milano, R. J., Bignell, G. R., Tam, A. T., Davies, H., Stevenson, J. A., Barthorpe, S., Lutz, S. R., Kogera, F., Lawrence, K., McLaren-Douglas, A., Mitropoulos, X., Mironenko, T., Thi, H., Richardson, L., Zhou, W., Jewitt, F., Zhang, T., O'Brien, P., Boisvert, J. L., Price, S., Hur, W., Yang, W., Deng, X.,

Butler, A., Choi, H. G., Chang, J. W., Baselga, J., Stamenkovic, I., Engelman, J. A., Sharma, S. V., Delattre, O., Saez-Rodriguez, J., Gray, N. S., Settleman, J., Futreal, P. A., Haber, D. A., Stratton, M. R., Ramaswamy, S., McDermott, U. & Benes, C. H. Systematic identification of genomic markers of drug sensitivity in cancer cells. *Nature* **483**, 570–575 (2012).

41. Lawrence, M. S., Stojanov, P., Mermel, C. H., Robinson, J. T., Garraway, L. A., Golub, T. R., Meyerson, M., Gabriel, S. B., Lander, E. S. & Getz, G. Discovery and saturation analysis of cancer genes across 21 tumour types. *Nature* **505**, 495–501 (2014).